Review

Journal of the Brazilian Chemical Society

https://dx.doi.org/10.21577/0103-5053.20260098

J. Braz. Chem. Soc. **2026**, *37-Spe2*, e-20260098, 1-28

First-Row (3d) Metal Catalysis in Aromatic Systems: Toward Late-Stage C–H Functionalization of Complex Molecules

Lívia C. R. M. da Frota *,[a]

[a]*Instituto de Química, Universidade Federal do Rio Grande do Sul, 91901-570 Porto Alegre-RS, Brazil*

Late-stage functionalization (LSF) has emerged as a powerful strategy for the direct modification of structurally complex molecules, enabling rapid access to valuable analogues and offering a step- and resource-economical platform for molecular diversification. Transition-metal catalysis has played a central role in advancing these transformations. However, to date, late-stage metal-catalyzed C–H functionalization has relied predominantly on noble transition metals. First-row (3d) transition metals are more abundant, less expensive, and generally less toxic, making them attractive alternative for sustainable LSF applications. In addition, they offer complementary reactivity to their noble metal congeners. This review focuses in the intersection of 3d-metal catalysis, C–H activation, and late-stage functionalization, with particular emphasis on the modifications of aromatic systems in complex molecules. A critical analysis of the key challenges associated with the use of 3d metals in these transformations, including issues related to catalyst reactivity and stability, as well as the chemo- and regio-selectivity is provided. By examining the advancements and limitations over the past decade, this review aims to offer insights into emerging strategies to overcome these challenges and to guide the development of more efficient and sustainable methodologies in transition-metal catalyzed C–H functionalization.

Keywords: 3d metals, C–H activation, late-stage functionalization, sustainable chemistry, transition metals

1. Introduction

Late-stage functionalization (LSF) has attracted significant attention as a strategy for the direct transformation of structurally complex molecules. It has been defined as "a desired chemoselective transformation on a complex molecule to provide at least one analogue in sufficient quantity and purity for a given purpose without the necessity for installation of a functional group that exclusively serves the purpose to enable said transformation".[1] Given that all complex molecules contain aliphatic and/or aromatic C–H bonds, the direct functionalization of these bonds offer clear advantages over classical approaches, which often rely on lengthy, resource-consuming synthetic sequences. In this context, C–H activation provides a time- and labor-saving platform for molecular diversification, particularly in drug development processes.[2-6]

Transition-metal catalysis has emerged as a powerful tool for enabling such transformations, offering rapid access to diverse analogues of complex molecular scaffolds. Nevertheless, achieving site-selective activation of a specific C–H bond within a multifunctional molecule remains a central challenge.[5] This issue is commonly addressed using directing groups,[7-11] which can either be inherent to the substrate or installed prior to the transformation. While the strict definition of LSF typically encompasses only the former scenario, excluding strategies that require pre-installed directing groups is not always practical. Indeed, even when a removable directing group must be introduced, C–H activation strategies that enable efficient diversification of complex molecules without making use of *de novo* synthesis, arguably fall within the broader conceptual framework of LSF, particularly when they provide cost-effective and step-economical access to valuable analogues.

Late-stage metal-catalyzed C–H functionalization has relied extensively on noble transition metals, especially palladium.[5,6,12] However, concerns regarding their low natural abundance and high cost together with the growing demand for sustainable chemical processes, have driven interest in the use of earth-abundant 3d transition metals. First-row transition metals are generally better tolerated as residual impurities in pharmaceutical compounds and

*e-mail: livia.frota@ufrgs.br
Editor handled this article: Emilio Carlos de Lucca Júnior (Guest)

play essential roles in numerous biological processes,[13,14] which combined with their greater abundance, make them particularly attractive for LSF applications. Despite these advantages, 3d-metal catalysts often exhibit lower stability and distinct reactivity profiles compared to their 4d and 5d counterparts,[14-16] which can limit their performance, particularly under mild conditions required for LSF. To address these challenges, significant efforts have been made to the development of suitable ligands and directing groups, as well as the use of additives capable of enhancing the reactivity and selectivity of 3d-metal-catalyzed C–H activation processes.

Several reviews published over the past decade have addressed those topics. However, most focus predominantly on noble metals,[2,5,13] particularly palladium, while those covering 3d metals are generally limited either to a single metal or to transformations involving small molecules.[2,17-20] In this review, aromatic C–H activation methodologies based on 3d metals (Mn, Fe, Co, Ni and Cu) reported over the past decade will be discussed. Although transition-metal catalyzed arene C–H functionalization can occur without arene-metal bond formation,[21-23] only processes involving the proposed formation of a metal-carbon bond during the catalytic cycle will be discussed. Emphasis is placed on the reactivity patterns associated with each metal and the nature of the key intermediates involved. Only studies that includes at least one example of C–H activation applied to the LSF of aromatic systems, such as in drugs, natural products, and biomolecules are considered. Selected examples also encompass cases in which C–H activation occurs in a simpler substrate that is subsequently coupled with a structurally complex coupling partner, thereby illustrating both the scope and limitations of these methodologies.

The aim of this review is to provide a critical assessment of the challenges associated with the use of 3d metals in the C–H functionalization of complex aromatic structures, with particular attention to catalyst reactivity, stability, and site- and chemo-selectivity. By examining these aspects, this review seeks to offer insight into current limitations and to highlight emerging strategies for overcoming them in the development of sustainable transition-metal catalyzed methodologies.

2. Manganese Catalysis

Among first-row (3d) transition metals, manganese exhibits the broadest range of accessible oxidation states. Nevertheless, most of its organometallic chemistry in catalysis is dominated by Mn^{I} and Mn^{II} species. Mn^{II} complexes are generally characterized by pronounced ionic character and high reduction potential, often displaying behavior reminiscent of Grignard-type reagents.[24,25] Higher valent manganese species have been predominantly employed in the activation of relatively weak C(sp^3)-H bonds, particularly those at secondary, tertiary and benzylic positions.[26,27]

Activation of the thermodynamically more stable aromatic C(sp^2)-H bonds, however, is typically achieved using Mn^{I} catalysts, which are commonly stabilized by strong π-acceptor ligands such as carbon monoxide.[27,28] These transformations frequently operate via chelation-assistance mechanisms involving directing groups and a migratory insertion within an overall redox-neutral fashion.[29,30] Because of these characteristics, over the past decade, examples of Mn-catalyzed aromatic C–H activation for late-stage functionalization have primarily focused on alkenylation reactions, with comparatively fewer reports for alkynylations and alkylation processes.

Manganese-catalyzed addition of aromatic C–H bonds to π-systems represents a hallmark transformation in Mn catalysis.[31] In 2017, Ackermann *et al.*[32] exploited this reactivity in the site-selective C2 alkynylation of indoles **1** using haloalkynes (**2**) (Scheme 1, top left). The scope of haloalkynes proved broad, encompassing silyl-substituted alkynes as well as aryl-, alkenyl- and alkyl-substituted variants, including complex alkynes derived from steroids and amino acids. Mechanistic studies indicated that the Mn^{I} catalyst enables rapid and reversible base-assisted C–H activation directed by an *N*-2-pyrimidyl group. In cases where the alkyne coupling partner lacked a silyl substituent, catalytic amounts of BPh_3 were required to facilitate the β-bromide elimination, thereby regenerating the alkyne functionality after migratory insertion into the Mn–C bond (Scheme 1, bottom left). Importantly, this methodology was successfully applied to the late stage alkynylation of tryptophan residues in short peptides and to the synthesis of cyclic peptides, highlighting its utility in the modification of biomolecules.

Shortly thereafter, the same group extended this Mn^{I}-catalyzed C–H activation strategy to the alkenylation of indoles using terminal alkynes bearing β–O leaving groups (**3**) (Scheme 1, top right),[33] thereby expanding the scope of coupling partners for hydroarylations.[31] In this transformation, the addition of a Brønsted-acid accelerates the protodemetallation step (Scheme 1, bottom right) and suppressed undesired β–O elimination pathways (Scheme 1, detail). The method was efficiently applied to the functionalization of protected tryptophan in 83% yield with complete *E*-selectivity, although no additional examples of late-stage functionalization were reported. Notably, the protocol was also adapted to continuous-flow conditions (Scheme 1, middle), enabling the site selective

C–H activation/hydroarylation of protected tryptophan within only 20 min.

Minor modifications to the reaction conditions enabled the extension of these methodologies to different protocols for the late-stage diversification of peptides (Figure 1). In 2021, the group of Ackermann *et al.*[34] reported the Mn^{I}-catalyzed, carboxylate-assisted C–H activation strategy for the hydroarylation of complex peptides with propiolates (**4**) (Figure 1a). This approach enabled the efficient conjugation of peptides to structurally complex biomolecules, including natural products and sugars, while maintaining broad functional group tolerance. Furthermore, the methodology was applied to the synthesis of cyclic peptides exhibiting anticancer activity (Figure 1, bottom). Importantly, the authors demonstrated the feasibility of removing the directing group from cyclic peptide products, highlighting the synthetic practicality of this approach to late-stage functionalization strategies.

In the same year, these strategies were further applied to the labeling of complex peptides with BODIPY fluorophores (**5** and **6**). The fluorophores bearing alkenyl or alkynyl linkers, which are key structural elements for tuning the photophysical properties of the probes, were introduced through Mn^{I}-catalyzed C–H activation followed by either alkynylation or hydroarylation (Figure 1b).[35] Notably, the authors demonstrated that a tryptophan-lauric acid derivative labeled with a BODIPY fluorophore bearing an alkene linker (Figure 1, bottom) functioned as a fluidity-sensitive probe, exhibiting fluorescence in response to subtle changes in the cholesterol content of cell membranes.

This Mn^{I}-catalyzed C–H activation of the indole core was also applied to the alkenylation of peptides with terminal alkynes bearing a nitrobenzodiazole (NBD) fluorophores (**7**) (Figure 1c).[36] Notably, in contrast to previously reported protocols employing Brønsted-acid additives, the use of the Lewis acid BPh_3 was essential for promoting the transformation, affording the alkenylated products with complete *E*-diastereoselectivity. Furthermore, the authors prepared an NBD-labeled peptide that exhibits turn-on fluorescence upon binding to microbial cell envelop, enabling wash-free imaging of bacterial cells (Figure 1, bottom). These findings highlight the potential of Mn-catalyzed late-stage functionalization as a platform for the development of fluoresce-based tools to investigate cell function. A related Mn-catalyzed C–H alkenylation strategy was also employed for the synthesis of alkenylcarborane-labeled[37] (Figure 1d) and coumarin- and chromone-labeled[38] tryptophan-containing small peptides with excellent

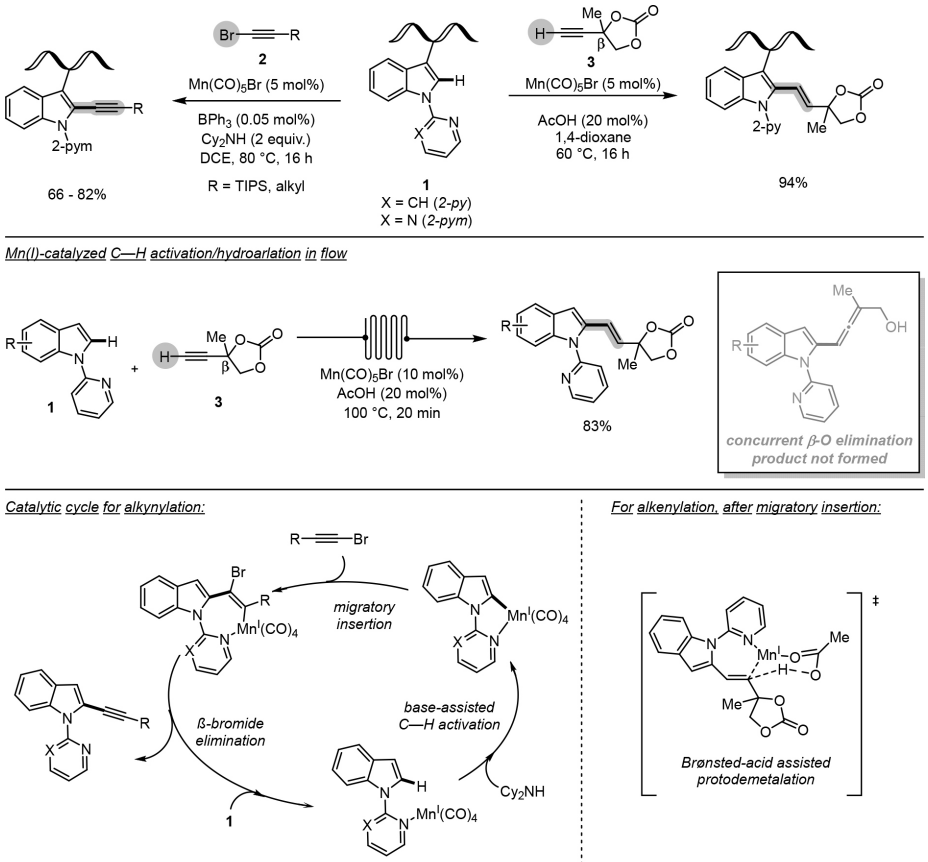

Scheme 1. Mn-catalyzed akynylation and alkenylation of indoles.

E-stereoselectivity (> 20/1), further demonstrating the versatility of Mn catalysis for the incorporation of different functional probes into peptides.

Although the 2-arylindazole motif is not commonly found in naturally occurring compounds, it is prevalent in numerous biologically active molecules, including marketed drugs, and has also been employed as fluorescent probes due to its favorable photophysical properties.[39,40] Thus, the development of C–H activation strategies targeting this scaffold is of significant synthetic interest. These strategies can be differentiated into two general categories: guided and innate. The former involves the coordination of the metal to a directing group, whether permanently or transiently attached to the substrate, which brings the metal to the proximity of the targeted C–H bond, selectively triggering its activation. In contrast, the latter relies exclusively on the intrinsic reactivity of the substrate and electronic or steric properties.[41] Most transition metal-catalyzed C–H activation methodologies involving 2-arylindazoles and related pyrazoles rely on their innate reactivity when d^8 metals, such as Pd^{II} are employed.[42] In contrast, the use of d^6 metals, particularly high-valent Lewis acidic Rh^{III} and Ru^{II}, enables indazole-directed *ortho*-C–H activation through formation of chelation-stabilized metallacycles, thereby providing complementary site selectivity.[42,43]

In this context and aligned with the development of more sustainable methodologies using earth-abundant 3d metals, Hajra *et al.*[44] reported the Mn^{I}-catalyzed indazole-directed C–H alkenylation of arenes with alkynes in water (Scheme 2). Based on the common reactivity of Mn^{II} via chelation-assistance mechanisms,[29,30] this strategy enabled the incorporation of 2-arylindazole (**9**) scaffold into structurally complex alkynes (**10**), including those derived from steroid and amino acids. Although the methodology was not extended to more complex peptide substrates, the use of aqueous reaction conditions combined with the successful coupling of amino acids-derived alkynes highlights its potential applicability for the late-stage modification of more complex peptide-based systems under biologically compatible conditions.

Besides alkynes, alkenylation reactions can also be accomplished using allenes as coupling partners in Mn^{I}-catalyzed C–H activation of indole C2 position.[45] In 2023, Almendros and Cembellín[46] reported the Mn^{I}-catalyzed insertion of acetylated allenes (**11**) into the C2–H bond of indoles (**1**), furnishing conjugated dienes (**12**) as products. Following C–H activation, migratory insertion of the C–Mn bond into the less hindered terminal double bond of the acetylated allene furnished complex **I**, in which coordination of Mn to the acetate group stabilizes the catalyst. Subsequent protodemetalation afforded an allylic acetate intermediate

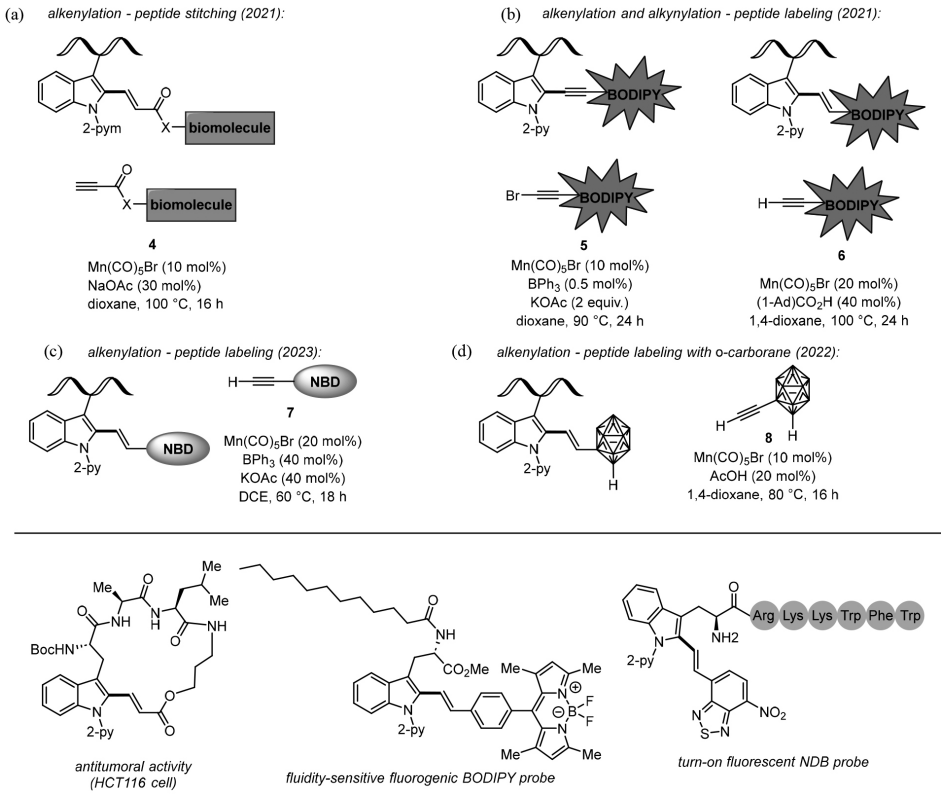

Figure 1. Late-stage functionalization of biomolecules employing the Mn^{I}-catalyzed C–H activation strategies.

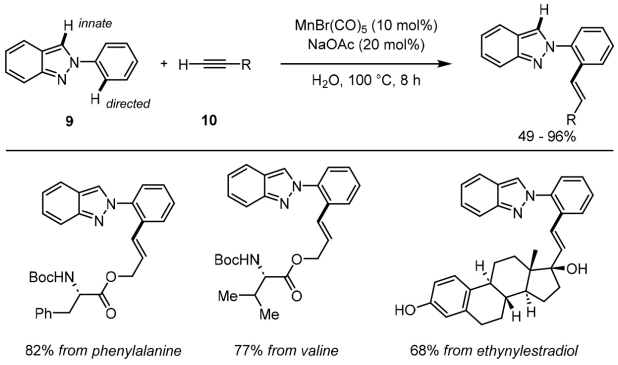

Scheme 2. Indazole-assisted Mn^{I}-catalyzed C–H alkenylation under aqueous conditions.

that, in the presence of 1,8-diazabicyclo[5,4,0]undec-7-ene (DBU), generated the conjugated diene, which likely undergoes isomerization through a Mn^{I}-mediated process,[47] delivering exclusively the linear C2-alkenylated indole products with high regioselectivity. Importantly, the transformation could be extended to other (hetero)aromatic substrates, including pyrrole and arenes bearing a pyridine directing group. This methodology was successfully applied in the functionalization of biomolecules-derived indoles such as melatonin, as well as to allenes derived from glyceraldehyde (Scheme 3). However, the scope with respect to more complex substrates remained limited, and no additional examples involving highly functionalized biomolecules were reported.

Mn-catalyzed allylation and alkylation reactions remain comparatively less developed than their alkenylation counterparts. Reported examples on Mn-catalyzed aromatic C–H allylation predominantly rely on activated olefins bearing a β-leaving groups (Scheme 4, right). In 2017, Ackermann *et al.*[48] described the Mn^{I}-catalyzed C2 allylation of indoles (**1**) using vinyl dioxolanones (**13**) as coupling partners. While the reaction proceeded efficiently in dioxane, enhanced diastereoselectivity favoring the *E* double bond was observed in polar protic solvents, such as trifluoroethanol (TFE) and water, an aspect particularly attractive for the late-stage functionalization of biomolecules, such as peptides, proteins and nucleic acids, which are generally soluble in water and protic solvents. Moreover, the strong hydrogen-bonding and metallic cation stabilizing ability of fluorinated alcohols can facilitate electrophilic C–H activation processes. In addition, their protic yet non-nucleophilic character enables compatibility with sensitive functional groups commonly found in complex molecules.[49] Under the optimized reaction conditions, tryptophan derivatives bearing either pyridinyl or pyrimidinyl directing groups were successfully functionalized without detectable racemization (Scheme 4).

In the same year, Zhang *et al.*[50] reported a related Mn^{I}-catalyzed difluoroallylation of **1** using bromodifluoropropene **14** under similar reaction conditions. Notably, tryptophan and melatonin analogues were also

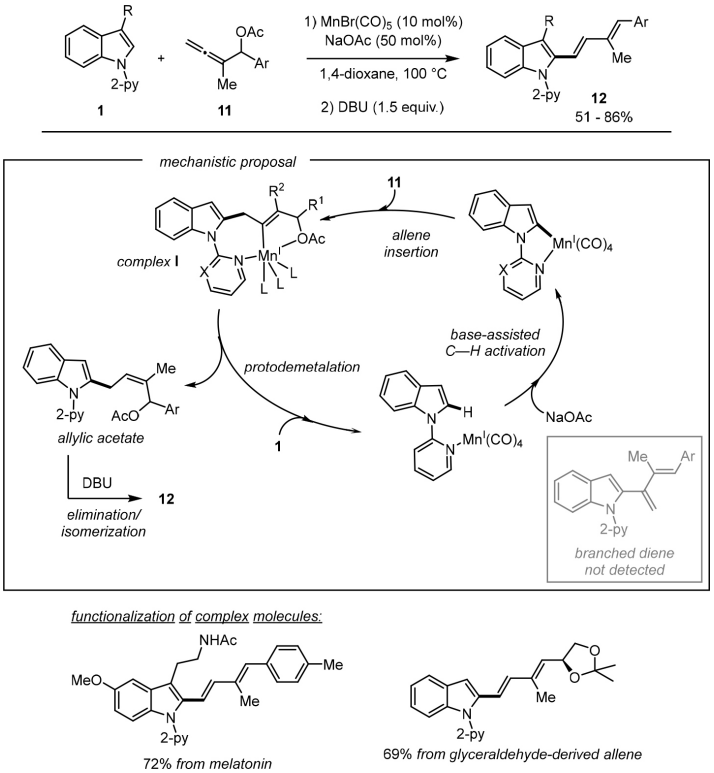

Scheme 3. Mn^{I}-catalyzed indole C–H insertion into allenes.

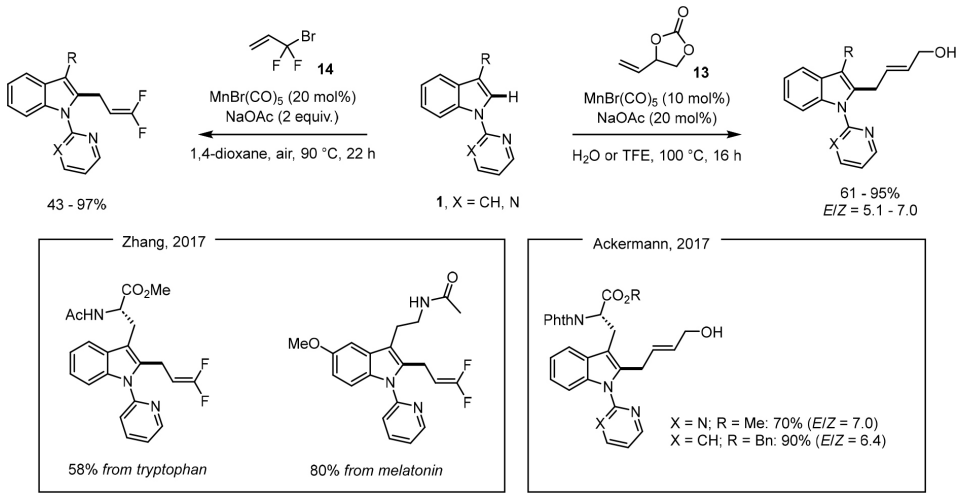

Scheme 4. Strategies to Mn^{I}-catalyzed C–H allylation of indoles C2 position.

amenable to this transformation (Scheme 4, left). In both studies, the mechanism is proposed to involve a fast and reversible chelation-assisted Mn^{I}-catalyzed C–H activation step, followed by a migratory insertion and subsequent β-elimination to furnish allylated products.

The application of this strategy to structurally more complex biomolecules was further advanced by Ackermann[51] in 2019 (Scheme 5). The chemoselectivity of the methodology was demonstrated through the functionalization of the indole core (**1**) of tryptophan within peptides containing free nucleophilic side chains, such as those in serine and tyrosine, electrophilic halide functionalities, and even oxidation-sensitive methionine residues. Moreover, the modified tryptophan amino acid was successfully coupled with a nucleophilic cysteine, highlighting the utility of this Mn^{I}-catalyzed approach in peptide ligation strategies (Scheme 5). The methodology also enabled the incorporation of structurally complex natural products-derived α,β-unsaturated esters into peptide scaffolds. Notably, purine was shown to serve as an effective directing group in this Mn^{I}-catalyzed C–H activation manifold, further demonstrating its potential for the late-stage functionalization of nucleoside analogues. Recently, the same group demonstrated the viability of this Mn^{I}-catalyzed C–H allylation protocol in biologically compatible aqueous reaction media.[52]

Metal-catalyzed C–H alkylation reactions employing alkyl halides are often challenging due to competing β-hydride elimination pathways. In this respect, manganese offers a distinct advantage as its organometallic intermediates display a reduced propensity to undergo β-hydride elimination.[29,30] Nevertheless, reported examples of manganese-catalyzed C–H alkylation with alkyl halides typically rely on excess strong bases, such as Grignard reagents,[53,54] which generally limits their applicability in late-stage functionalization.

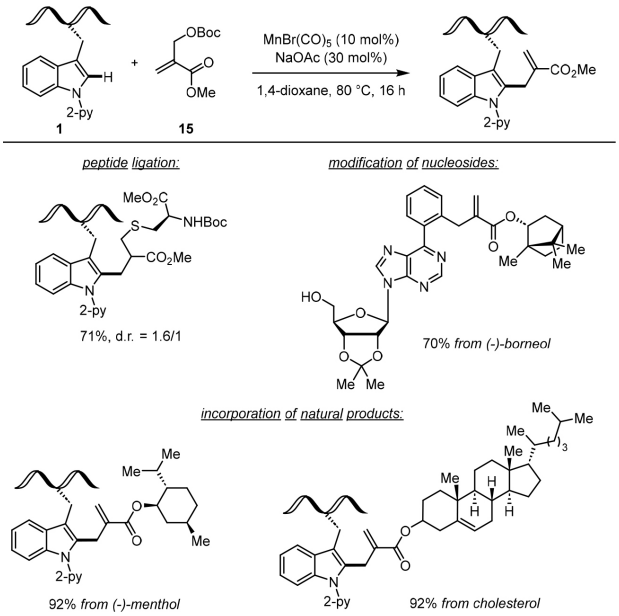

Scheme 5. Mn^{I}-catalyzed C–H allylation of C2 position of tryptophan residues within peptides and purine-assisted Mn-catalyzed arene C–H allylation of nucleosides.

Punji *et al.*[55] demonstrated that the use of a less nucleophilic base such as lithium bis(trimethylsilyl) amide (LiHMDS) instead of a Grignard reagent, allowed a ligand-free chelation-assisted Mn^{II}-catalyzed C–H activation strategy to be combined with alkyl halides (**16**) to promote alkylation. Mechanistic studies suggest that the reaction proceeds through a rate-determining Mn^{II}-catalyzed C–H activation step followed by oxidative addition of the alkyl halide through a radical pathway. A range of primary linear and branched alkyl bromides bearing different chain length were suitable coupling partners. However, shorter chains generally afforded higher yields, which was attributed to their improved solubility in the reaction solvent. This approach allowed the incorporation of natural product-derived halides,

including thymol and structurally complex cholesterol derivatives (Scheme 6). Despite the tolerance toward various functional groups in both coupling partners, the substrate scope remains largely restricted to primary alkyl bromides and is incompatible with base-sensitive functionalities such as carbonyl groups, which limits its broader application in late-stage functionalization.

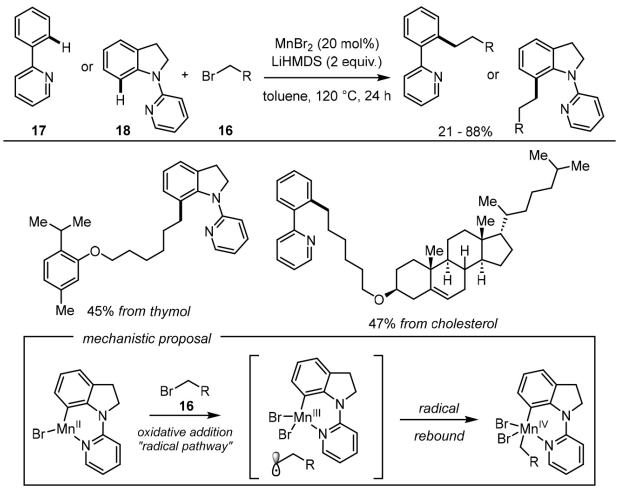

Scheme 6. Mn^{II}-catalyzed C–H alkylation with alkyl halides.

3. Iron Catalysis

Iron, the most abundant transition metal on the crust of Earth, exhibits a wide range of accessible oxidation states varying from –2 to +6, enabling diverse reactivity in C–H activation processes.[56] Such transformations typically proceed with the assistance of a directing group and involve either low- or high-valent iron intermediates. In systems using high-valent Fe^{II} or Fe^{III} in combination with strongly coordinating directing groups, C–H activation commonly occurs via a σ-bond metathesis pathway. In contrast, low-valent Fe^0 species, particularly combined with weakly coordinating directing groups, can promote oxidative addition into *ortho* C–H bonds.[56-58] Alternatively, both high- and low-valent Fe species may engage in ligand-to-ligand hydrogen transfer pathways for C–H activation.[59-62] Owing to the high reactivity of organoiron intermediates, these transformations must be performed under comparatively lower temperatures relative to analogous processes catalyzed by 4d and 5d metals. This feature, combined with low toxicity of iron and high natural abundance,[13] renders it an attractive catalyst for late-stage functionalization, particularly in the context of biomolecules. Despite these advantages, reports on Fe-catalyzed C–H activation applied to late-stage functionalization remain scarce, with only a limited number of examples disclosed over the past decade.

Recently, Ackermann *et al.*[60] reported a regioselective C–H alkylation of indoles bearing a weakly coordinating *N*-PMP directing group (**19**) with alkenes (**20**), enabled by a three-coordinated Fe^0 catalyst (**21**) (Scheme 7). The use of this Fe^0 complex supported by a *N*-heterocyclic carbene (NHC) ligand allowed the transformation to proceed at room temperature and in the absence of Grignard reagents as bases, affording the products with exclusive Markovnikov selectivity. In contrast, the use of vinylsilanes led to anti-Markovnikov selectivity, likely due to steric repulsion between the silyl and *p*-methoxylphenyl (PMP) groups during C–H activation step. A related Ru-catalyzed reaction exhibited the same regioselectivity but required refluxing toluene to achieve

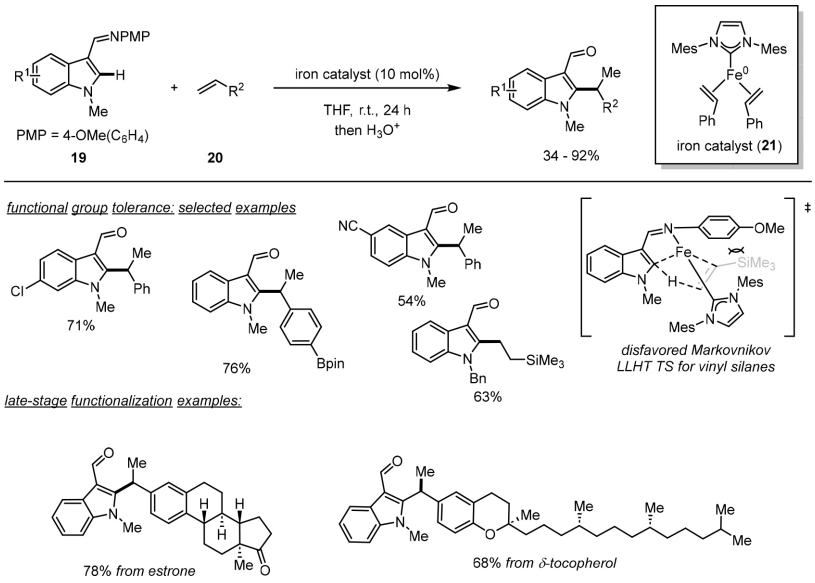

Scheme 7. Fe^0-catalyzed C–H alkylation of indoles with the assistance of a weakly coordinating directing group.

comparable yields.[63] In contrast, palladium-catalyzed C–H activation methodologies applied to related indole systems exhibit different regioselectivity, promoting activation at C4 position rather than at C2.[64] The protocol exhibits good functional group tolerance, accommodating styrenes bearing boronate esters as well as indoles containing base-sensitive functionalities, such as a cyano groups. Mechanistically, the authors proposed that C–H activation proceeds via a ligand-to-ligand hydrogen transfer (LLHT) pathway, which is favored over concerted oxidative additions for low-valent 3d metals due to their smaller atomic radii and lower M-H bond dissociation energies relative to their 4d and 5d congeners.[59] Although only two examples of late-stage modification were demonstrated, the mild reaction conditions avoiding Grignard reagents highlight the potential of this methodology to broaden the scope of iron-catalyzed C–H functionalization, particularly for late-stage modification of complex biomolecules.

C–H allylation using allenes has already been demonstrated for indole scaffold bearing nitrogen heterocyles as directing groups, affording *Z*-alkenes under Mn catalysis.[65] More recently, Ackermann *et al.*[61] reported a Fe^{II}-catalyzed C–H allylation of benzamides (**22**) with allenes (**23**), enabled by a bidentate triazolyl directing group, delivering *Z*-alkenes with exclusive selectivity (Scheme 8). Density functional theory (DFT) studies suggested that the C–H activation proceeds via a ligand-to-ligand hydrogen transfer mechanism, while subsequent allene coordination and migratory insertion into Fe^{II} center constitute stereodetermining step, with steric repulsion favoring formation of the *Z*-alkene. Despite requirement for excess Grignard reagent as base, the reaction proceeded under relatively mild conditions, being effective even at room temperature. The protocol exhibits good functional group tolerance, accommodating sensitive functionalities such as boronates, halogens, esters and nitriles. Furthermore, the triazolyl directing group can be readily removed under mild conditions, although this was primarily demonstrated for less complex substrates. The methodology was successfully applied to the functionalization of structurally more complex allenes derived from natural products, biomolecules and even a supramolecular calix[4]arene scaffold, underscoring its potential for late-stage diversification strategies.

4. Cobalt Catalysis

Compared with their 4d and 5d counterparts, cobalt organometallic species are generally more nucleophilic due to lower electronegativity of cobalt, which enables distinct reactivity patterns and selectivity profiles.[66] Early examples of cobalt-catalyzed C–H activation relied on Co^{I} species generated *in situ* from Co^{II} salts and Grignard reagent, which limited the substrate scope and practical applicability. Subsequent developments in the field have been enabled by using bench stable, high-valent cobalt complexes. In general, Co^{III}-catalyzed C–H activation proceeds through a concerted metalation-deprotonation (CMD) pathway assisted by monodentate directing groups, whereas bidentate ones are often required to stabilize the *in situ* formation of high-valent Co^{III} intermediates from Co^{II} salts under oxidative conditions.[67,68]

Over the past decade, numerous examples of Co^{III}-catalyzed C–H activation have been reported for

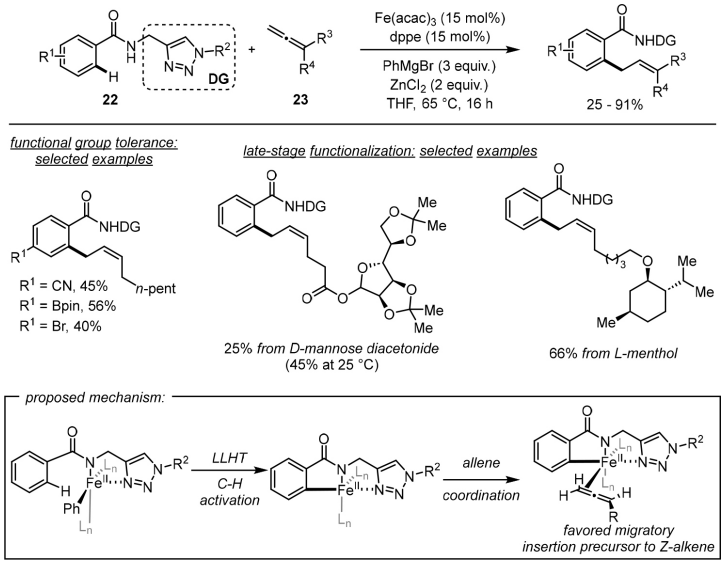

Scheme 8. Fe^{II}-catalyzed C–H allylation of benzamide bearing a triazolyl directing group using allenes as coupling partners.

late-stage functionalization applications. Most reported transformations involve cyclization or allylation reactions, although some examples of alkylation, a single example of arylation, and some multicomponent reactions have also been described.

In 2018, Sundararaju *et al.*[69] reported the synthesis of phthalimides (**24**) via Co^{III}-catalyzed C–H carbonylation of benzamides (**25**). The use of a bidentate 8-aminoquinoline directing group enabled the *in situ* generation of the active Co^{III} species from Co^{II} in the presence of Ag^{I} as oxidant. A two-chamber system was employed,[70] in which CO was generated from the reduction of CO_2 with tetramethyldiphenylsilane in one chamber and subsequently transferred to the second chamber, where the quelation-assisted Co^{III}-catalyzed C–H activation took place (Scheme 9). This strategy represents a significant advancement over earlier methodologies that relied on the direct use of CO gas,[71] thereby mitigating safety concerns associated with its toxicity and flammability. The protocol exhibits a broad substrate scope, delivering site-selective C–H carbonylation in good yields, even in the presence of strongly coordinating direct groups commonly found in pharmaceutical scaffolds, such as pyridine, pyrazine, and pyrazole. Furthermore, the methodology was successfully applied to the carbonylation of the angiotensin II receptor blocker telmisartan, highlighting its potential for site-selective late-stage functionalization.

A related Co^{III}-catalyzed protocol for the C–H carbonylation of phenylalanine derivatives (**26**) was later reported, employing picolinamide as a traceless directing group and CO gas as the carbonyl source, to afford dihydroisoquinolinolones (**27**) in good yields (Scheme 10).[72] The authors isolated and characterized a Co^{III} intermediate (**28**), providing strong support for a Co^{III}-catalyzed C–H activation pathway. The methodology was successfully extended to the modification of small di- and tri-peptides, highlighting its potential applicability to biomolecule late-stage functionalization. However, certain limitations were identified, including relatively high catalyst loadings and partial racemization of the substrates. Despite these drawbacks, the reaction exhibits a broad substrate scope and notable tolerance toward halide functionalities. Importantly, the products are obtained without the directing group, which is advantageous for applications requiring deprotected peptides derivatives.

In 2021, Gandon *et al.*[73] reported a Co^{III}-catalyzed double annulation of aryl thioamides (**29**) with alkynes (**30**), employing a *N*-masked thioamide as directing group for

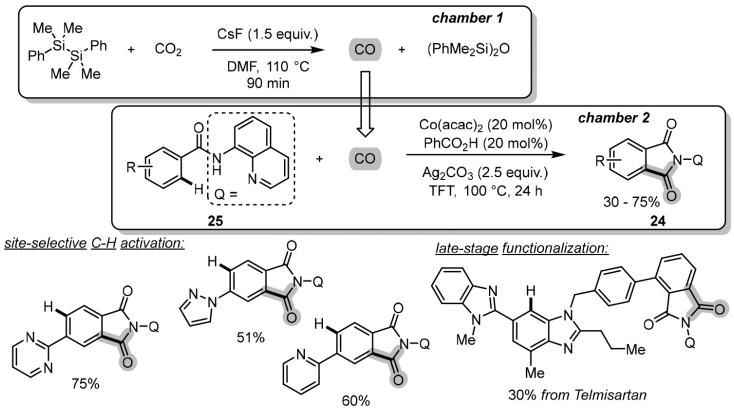

Scheme 9. Co-catalyzed C–H carbonylation of benzamides using a two-chamber strategy for CO generation. TFT: α,α,α-trifluorotoluene.

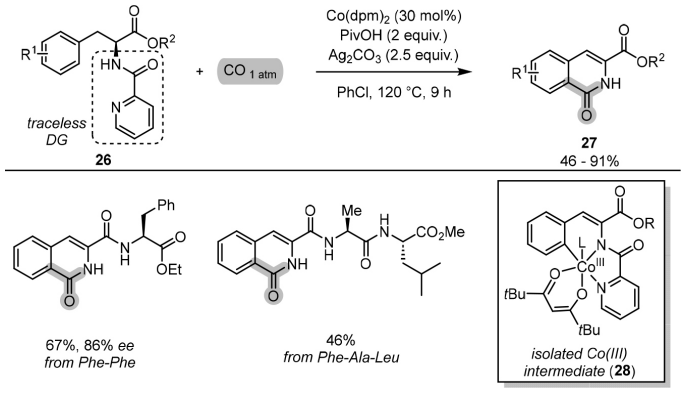

Scheme 10. Co-catalyzed C–H carbonylation of phenylalanine derivatives using a traceless directing group strategy.

C–H activation (Scheme 11). In contrast to previously reported methods using unprotected thioamide as directing group,[74,75] the *N*-methylphenyl sulfoximine (MPS) protecting group proved to be crucial for enabling the double annulation, as it promotes preferential *S*-coordination over *N*-coordination of cobalt catalyst to the thioamide. This coordination mode was supported by DFT studies and experimental observation of isothiochromenone (**31**) formation under hydrolytic conditions (Scheme 11, detail). These findings underscore the importance of rational directing group design in controlling regioselectivity in C–H functionalization. Notably, weakly coordinating functional groups, such as esters and ketones, were well tolerated, whereas strongly coordinating groups, including 2-pyridyl and 2-pyrazolyl, were not. Furthermore, a range of MPS-protected thiobenzamides derivatives bearing terpenoid motifs, as well as derivatives of marketed drugs, were successfully transformed using this methodology, highlighting its potential for increasing structural complexity in natural products and pharmaceutically relevant molecules.

Over the past decade, electrochemistry and photoredox catalysis have emerged as attractive, sustainable alternatives to stoichiometric oxidants in organometallic C–H activation, enabling the regeneration of high-valent metal catalyst from low-valent intermediates within the catalytic cycle.[76-78] Beyond this role, in Co-catalyzed C–H activation for late-stage functionalization, examples of these strategies in promoting the *in situ* generation of the active Co^{III} species from bench-stable Co^{II} precursors, typically in combination with bidentate directing groups, have been reported.

Recently, Dong *et al.*[79] reported the cobalt-catalyzed, 8-aminoquinoline-assisted electrochemical C–H activation/annulation of benzamides (**25**) with inactivated alkenes (**20**) (Scheme 12a). Under the reaction conditions, the active Co^{III} catalyst, generated via anodic oxidation of a Co^{II} precursor, promotes the C–H activation step via a base-assisted electrophilic substitution (BIES) pathway. Subsequently, a Co^{III}/Co^{I} catalytic cycle takes place, involving product-releasing reductive elimination from Co^{III} intermediate, while hydrogen evolution occurs as the cathodic process. The electrochemical activation of cobalt catalyst obviates the need for conventional stoichiometric oxidants such as Ag^{I} salts. The protocol exhibits a broad substrate scope and good functional group tolerance, including free alcohol and halides, such as bromine and chlorine. Notably, the methodology enables the efficient installation of dihydroisoquinolone (**32**) motifs into complex natural products, biomolecules, and pharmaceutical scaffolds. However, attempts to remove the directing group were unsuccessful, which may limit its applicability in late-stage functionalization when the directing group is not inherently present in the target molecule.

The allylation of benzamide **25** was also achieved through the merger of Co-catalyzed C–H activation with an eosin Y-mediated photoredox catalytic cycle, which serves as oxidant, using vinyl diazoacetates (**33**) as coupling partners (Scheme 12b).[80] In contrast to a previously reported Rh^{III}-catalyzed C–H activation of benzamide with vinyl diazoacetates,[81] the Co^{III} intermediate generated after diazo insertion exhibit exclusive vinylogous, rather than carbene, reactivity, affording the allylated products (**34**) selectively. The substrate scope is broad, with benzamides bearing halide functionalities being well tolerated. Although the method is limited to substrates containing terminal alkenes, vinyl diazo compounds bearing complex natural products motifs are compatible with the reaction conditions,

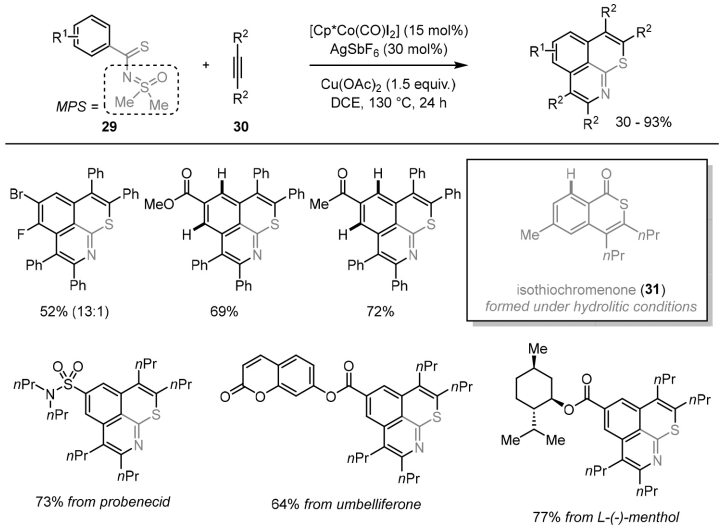

Scheme 11. Co-catalyzed double annulation of *N*-protected-thiobenzamide.

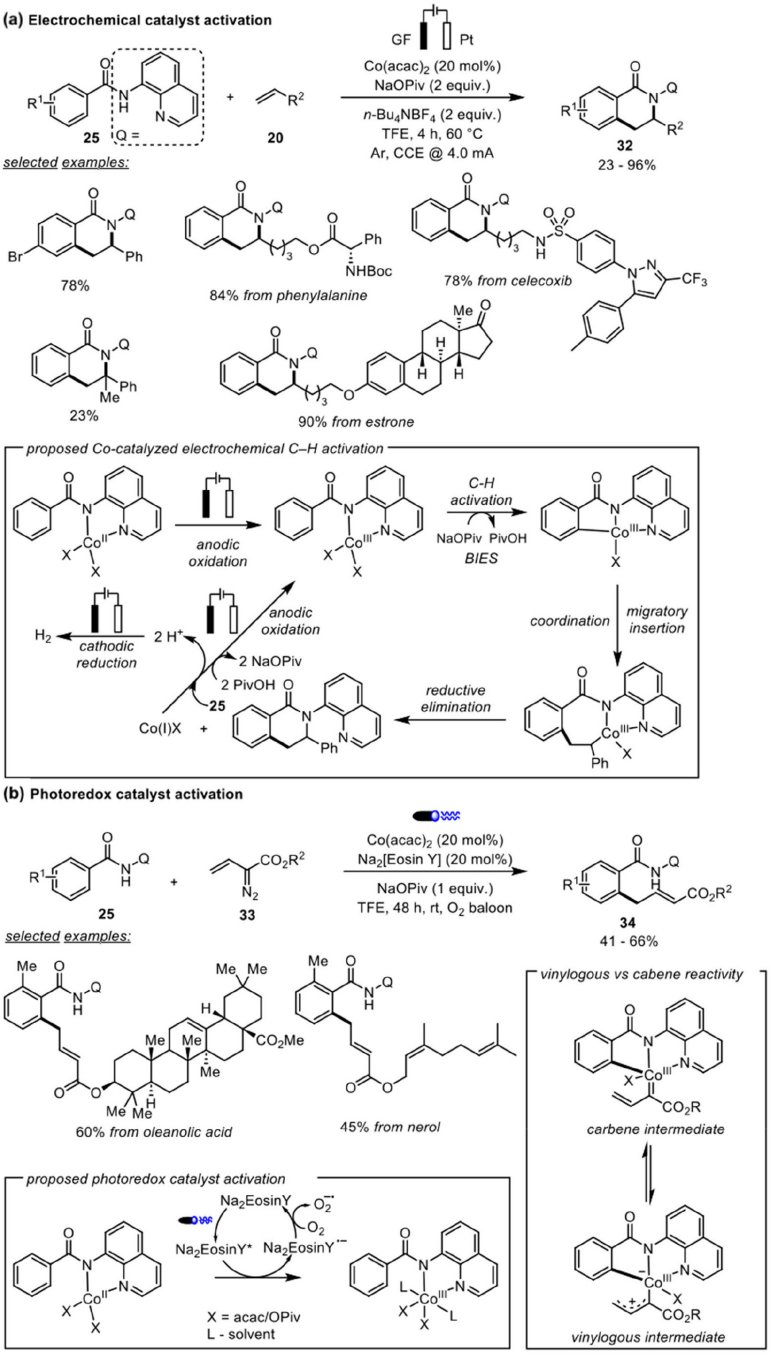

Scheme 12. Alternatives to stoichiometric oxidants in Co-catalyzed C–H activation. (a) Electrochemical activation, (b) photoredox activation.

highlighting the potential of this strategy for late-stage functionalization of complex molecules.

The allyl moiety is a highly versatile functional group that enables a wide range of subsequent transformations. Based on a related strategy using allyl carbonates as allylating agents, previously reported by Glorius *et al.*[82] developed a Co^{III}-catalyzed C–H activation of the indole scaffold (**1**) in tryptophan residues within complex peptides using allyl acetates (**35**) as coupling partners (Scheme 13, right).[83] Both pyridinyl- or pyrimidinyl-directing groups proved effective for chelation-assisted C–H activation and the reaction proceeded well even at room temperature. Moreover, a variety of protecting groups commonly used in peptide chemistry, as well as protic functional groups, including free peptidic NH, carboxamide and OH, were well tolerated with high chemoselectivity, highlighting the robustness and functional group compatibility of this methodology. Notably, this strategy was further applied to the synthesis of structurally complex cyclic peptides through a catalytic sequence combining C–H

functionalization, olefin metathesis and hydrogenation, thereby underscoring its potential to enhance step economy in cyclic peptide synthesis.

Shortly thereafter, Wei *et al.*[84] reported a related approach employing vinyl dioxanone (**36**) as a homoallylic alcohol surrogate (Scheme 13, left). The reaction proceeds under mild conditions, delivering products with high diastereoselectivity favoring the *E* double bond and exhibiting a broad functional group tolerance. Particularly, bromo and chloro substituents are well tolerated, enabling subsequent orthogonal cross-coupling transformations. Both pyrimidinyl- and pyridinyl-directing groups were compatible with the C–H functionalization protocol, with the former generally providing higher diastereoselectivity in substrate bearing substitution at the C3 position. The methodology was further extended to the late-stage functionalization of tryptophan and its derivatives, including melatonin and commercial drug zolmitriptan. DFT studies indicated that the diastereoselectivity arises from the olefin migratory insertion step of the catalytic cycle, which may account for the diminished selectivity observed in the late-stage functionalization of more sterically demanding indole derivatives.

In 2023, the Co^{III}-catalyzed C–H allylation of aryl sulfoxonium ylides (**37**) was accomplished using vinyl cyclopropanes (**38**) as allyl surrogates (Scheme 14).[85] In contrast to previously reported[86-89] transformations of (**37**) which generates carbenes with 4d and 5d group 9 metals, under cobalt catalysis the sulfoxonium ylide functions as a weakly coordinating directing group, enabling the *ortho*-C–H activation under mild conditions with excellent diastereoselectivity favoring the *E*-isomer. The methodology exhibits good functional group tolerance, notably accommodating halide substituents such as bromo and chloro groups. In addition to vinyl cyclopropanes, other strained allyl surrogates, including vinyl oxiranes, aziridines, and dioxolanes were also effective, providing the allylated products with comparable efficiency. Furthermore, the protocol was successfully applied to the late-stage modification of derivatives of commercial drugs such as probenecid and ataluren, demonstrating selective allylation at the position *ortho* to the sulfoxonium ylide over other potentially coordinating directing groups, such as sulfonamide and oxadiazole.

In 2020, Ackermann *et al.*[90] leverage the high electrophilicity of Co^{III} catalyst to promote chelation-

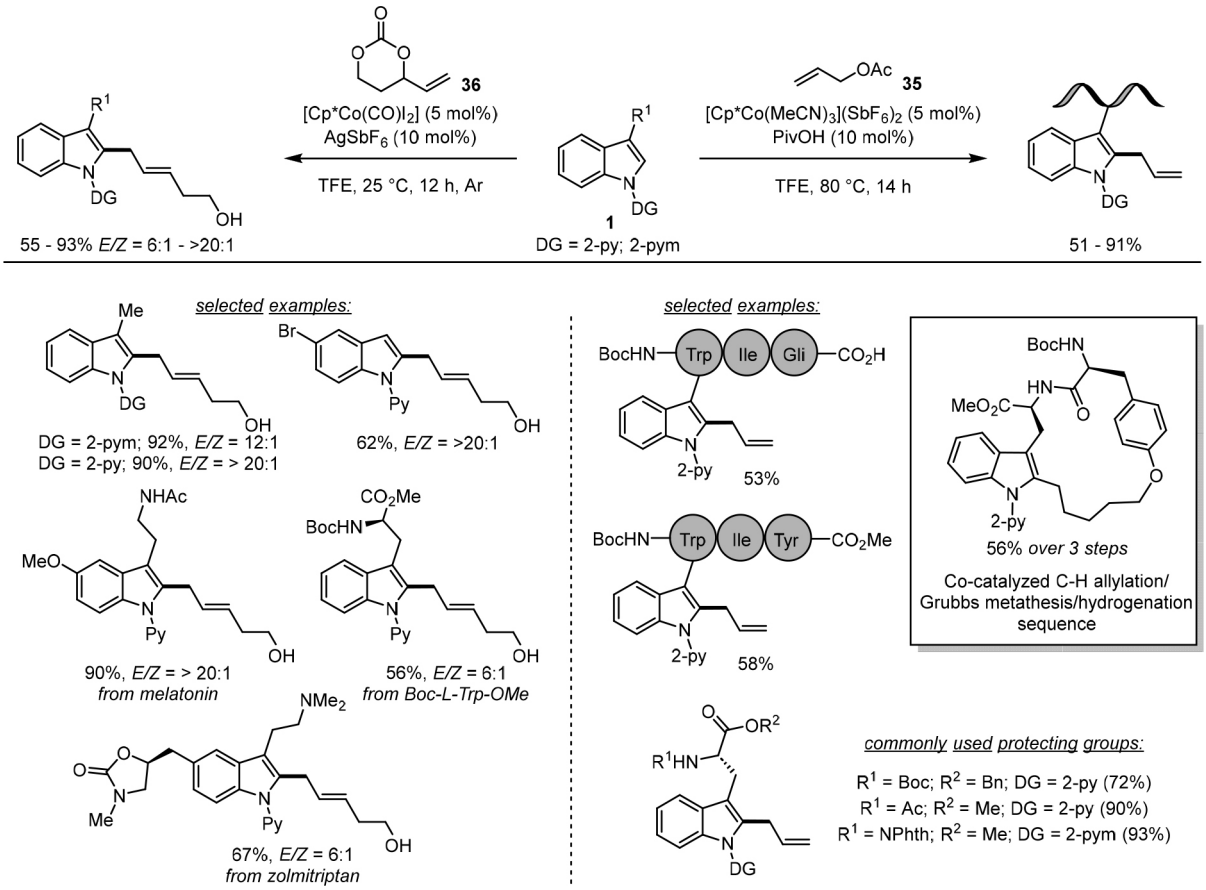

Scheme 13. Co-catalyzed C–H allylation of indole moiety. (Right) allylation of peptides with allyl acetate; (left) allylation of tryptophan and derivatives with vinyl dioxanone.

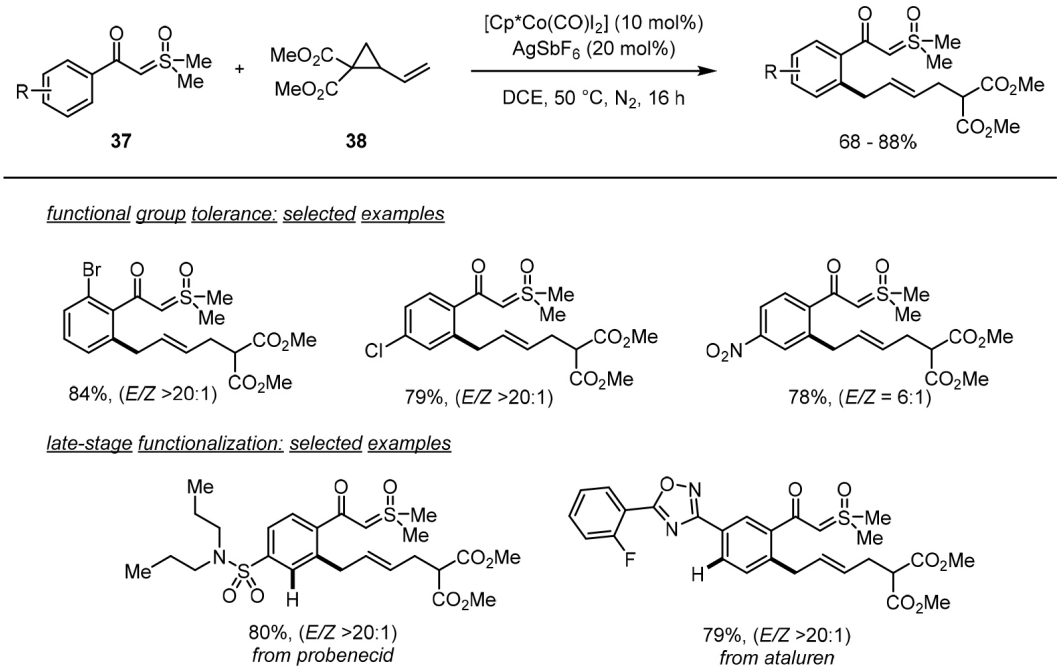

Scheme 14. Regioselective Co^{I}-catalyzed C–H allylation employing sulfoxonium ylides as directing group.

assisted C–H activation followed by an unprecedent transmetallation from a boron-based methyl source to the resulting metallacycle **I** (Scheme 15). High-throughput experimentation (HTE) was employed to systematically optimize reaction parameters, as well as to evaluate directing group reactivity and functional group tolerance, thereby delineating the scope and limitations of the methodology for late-stage methylation of bioactive molecules. The optimized conditions relied on the use of boroxine **39**, which are better alternatives to boronic acids under moisture-sensitive reaction conditions.[91,92]

The study assessed the directing ability of different groups commonly found in pharmaceuticals and structurally complex bioactive compounds, establishing a reactivity hierarchy that provides a practical guideline for predicting site-selectivity in late-stage methylation. In late-stage functionalization in substrates bearing multiple weakly coordinating directing groups, employing stoichiometric amounts of cobalt catalyst and excess boroxine improved the reaction yields while allowing

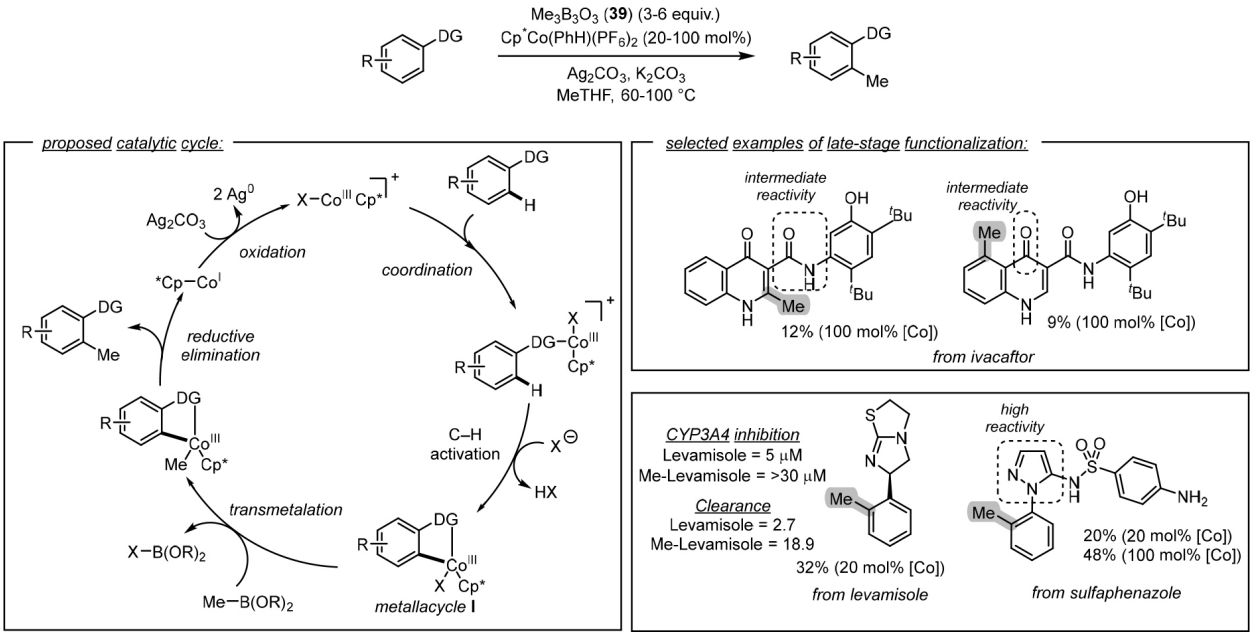

Scheme 15. Co-catalyzed methylation via transmetallation to boron-based methyl source and impact of methylation in pharmacokinetic properties.

recovery of intact starting material, which is particularly advantageous for functionalization of high-valued complex molecules. Nevertheless, site-selectivity remained challenging when multiple weakly-coordinating directing groups were suitably positioned for chelation, leading to mixtures of methylated products. Replacing a hydrogen atom with a methyl group in a molecule can significantly improve its biological or pharmacological properties through changes in molecular conformation, hydrophobic interactions, desolvation energetics, and metabolic stability. These phenomena are collectively referred to as the magic methyl effect and, in some cases, can lead to potency enhancements exceeding 1000-fold.[93] Notably, selected examples were used to demonstrate the impact of methylation on drug metabolization and pharmacokinetic properties, including clearance and cytochromes P450 (CYP450) inhibition (Scheme 15).

In the same year, Maji *et al.*[94] reported an alkylation strategy based on Co^{III}-catalyzed C–H activation followed by an acrylate (**40**) migratory insertion/protodemetallation sequence (Scheme 16a, right). Notably, this study demonstrated for the first time the use of *O*-carbamates as directing group in cobalt C–H activation. The addition of a Brønsted acid was found to favor protodemetallation over β-hydride elimination, suppressing the competing alkenylation pathway. Furthermore, switching the directing

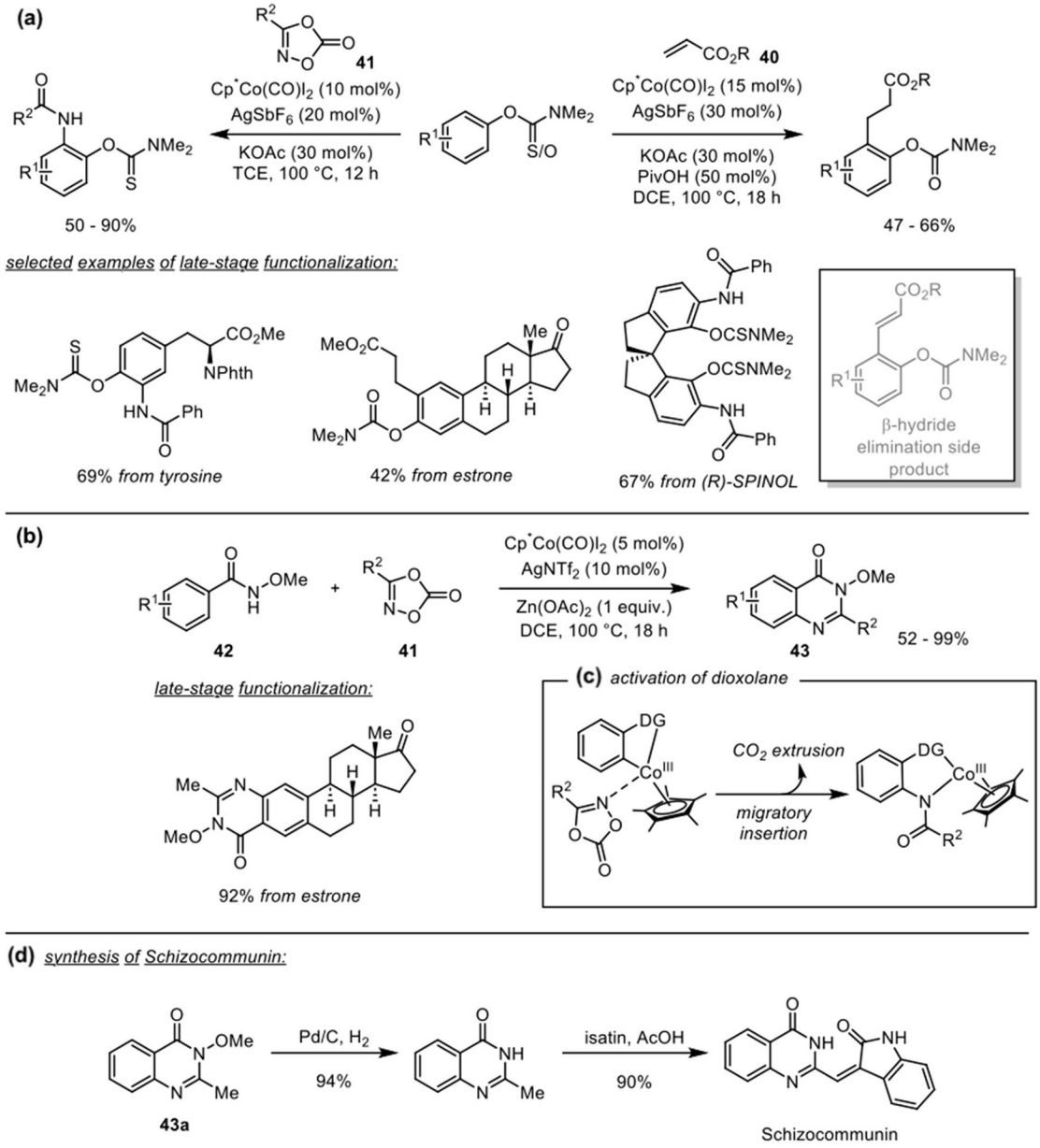

Scheme 16. Co-catalyzed C–H alkylation and amidation strategies. (a) *O*- and *S*-carbamates as directing groups, (b) amidation/cyclization sequence to quinazolines, (c) migratory insertion step, (d) synthesis of schizocommunin.

group from a carbamate to the more strongly coordinating thiocarbamate enabled C–H amidation using dioxolane (**41**) as the amide source (Scheme 16a, left). Interestingly, Liu *et al.*[95] previously reported a related strategy employing (**41**) and *N*-methoxybenzamide (**42**) as a nucleophilic directing group, leading to C–H amidation products that subsequently undergo Zn-mediated cyclization to afford quinazoline (**43**) scaffolds (Scheme 16b). The presence of sulfur facilitates migratory insertion of (**41**), likely via a pathway involving CO_2 extrusion (Scheme 16c).[96] Notably, removal of the OMe group from quinazoline (**43a**), obtained via Co-catalyzed C–H amidation, followed by acid-catalyzed condensation with isatin, efficiently furnished schizocommunin (Scheme 16d). Beyond natural product synthesis, those methodologies were also successfully applied to the functionalization of structurally more complex substrates, including tyrosine and estrone derivatives, as well as of BINOL and SPINOL frameworks, highlighting its potential utility in the synthesis and design of new chiral ligands and other value-added molecules.

The selective C8 alkylation of quinoline *N*-oxides (**44**) under Co^{III} catalysis was first reported in 2016 via a C–H activation/oxygen atom transfer sequence using internal alkynes, leading to the formation of α-functionalized ketones.[97] The high regioselectivity of electrophilic Co^{III} toward the C8 position of quinoline is likely due to its greater nucleophilicity compared to the more commonly functionalized C2 position.[98] Building on the weakly coordinating nature of the *N*-oxide group, Punniyamurthy *et al.*[99] subsequently developed a complementary strategy using cyclopropanols (**45**) as alkylating agents for the regioselective functionalization of quinoline derivatives under Co^{III} catalyst, affording β-substituted ketones (**46**) instead (Scheme 17). High resolution mass spectra (HRMS) analysis of the reaction mixture revealed the formation of Co^{III}-alkyl species (**47**) from β-carbon cleavage of the cyclopropanol ring, supporting the proposed C–H/C–C activation pathway. TFE was identified as the optimal solvent, likely due to its ability to stabilize high-valent cobalt intermediates involved in the C–H activation process, as well as to enhance catalyst solubility.[49,100] The protocol exhibits broad functional group tolerance, including halogen substituents such as bromine and iodine, thereby enabling subsequent orthogonal transformations. The methodology was successfully applied to late-stage functionalization of complex molecules, exemplified by a quinoline derivatives bearing gemfibrozil and sesamol motifs, as well as a cyclopropanol coupling partner derived from ibuprofen, underscoring its potential in the modification of pharmaceuticals and natural products.

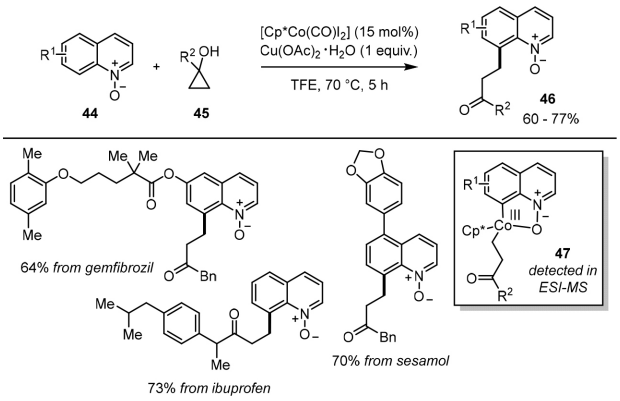

Scheme 17. Co-catalyzed C–H alkylation of quinoline *N*-oxides using cyclopropanol as coupling partners.

The merger of C–H activation strategies with multi-component reactions has the potential to improve synthetic sustainability by improving step economy while building molecular complexity. While most of the methodologies rely on noble transition metals, such as palladium, the use of inexpensive, less toxic 3d metals is still underdeveloped.[13,101,102]

In 2022, Koenig *et al.*[103] reported a Co-catalyzed three-component arene (**48**)-alkene (**49**)-alkyne (**50**) coupling that provides *ortho*-homoallylated arenes (**51**) under mild conditions (Scheme 18). The authors design a Co^{I} precatalyst (**52**) bearing a strongly electron-donating alkylphosphine ligand, which hampers the unimolecular β-hydride elimination or C–C reductive elimination pathways typically associated with Co^{III} metallacyclopentanes. Formation of the key Co^{III} intermediate (**53**) via oxidative cyclization with (**49**) and (**50**) is proposed to precede chelation-assisted C–H activation, as supported by control experiments, analysis of side-product profiles, and deuterium-labeling studies. A range of directing groups, including amide, ketone and pyridyl, was evaluated, with weakly coordinating groups generally providing better results, likely due to the enhanced reactivity of the high-valent Co^{III} intermediate generated after C–H activation. Although ethylene is the only alkene compatible with the reaction conditions, symmetrical alkynes bearing both alkyl and aryl substituents were well tolerated. Unsymmetrical alkynes also participated in the transformation, albeit affording mixture of regioisomers that preferentially place the smaller substituent at the terminal alkene position. The reaction exhibits good functional group tolerance, including bromo and boronic ester functionalities. The utility of this methodology for late-stage functionalization was further demonstrated by the modification of the commercial drugs fenofibrate and haloperidol. Overall, this work highlights the critical role of catalyst design in expanding the scope of metal-catalyzed C–H functionalization reactions.

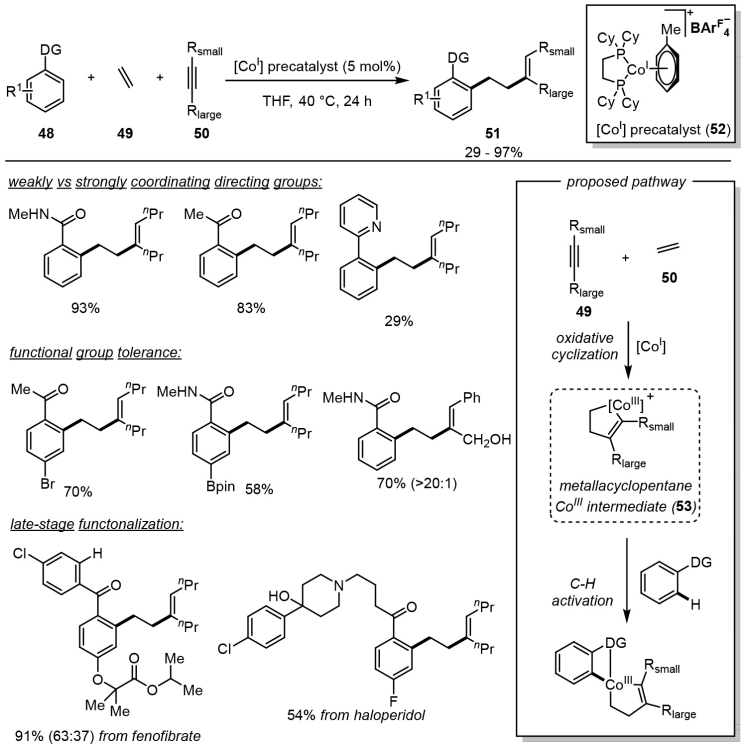

Scheme 18. Co-catalyzed three-component arene-alkene-alkyne coupling: *in situ* formation of Co^{III} active catalyst for C–H activation from Co^{I} precatalyst. $BArF^{4-}$: $B[(3,5\text{-}(CF_3)_2)C_6H_3]_4$.

Recently, Manolikakes *et al.*[104,105] reported the synthesis of *N*-sulfonyl amines (**54**) through a Mannich-like coupling combined with Co^{III}-catalyzed C–H activation (Scheme 19). In this protocol, the amine products are formed via a migratory insertion/protodemetallation sequence involving the *in situ* generated sulfonimine and a Co^{III} intermediate arising from pyridinyl-assisted C–H activation. Notably, the direct use of a cationic cobalt catalyst, rather than its conventional *in situ* generation from a neutral Co^{III} precursor in the presence of Ag^{I}, significantly improves reaction efficiency. The methodology displays good functional group tolerance, including halide functionalities. However, limitations were observed for substrates bearing *ortho* substitution in any of the three coupling partners, as well as the use of aliphatic aldehydes (**55**). Both 2-arylpyridines (**17**) and 2-pyrimidinylindoles (**1**) were efficiently coupled with the *in situ* generated sulfonamides. Furthermore, the applicability of this methodology to

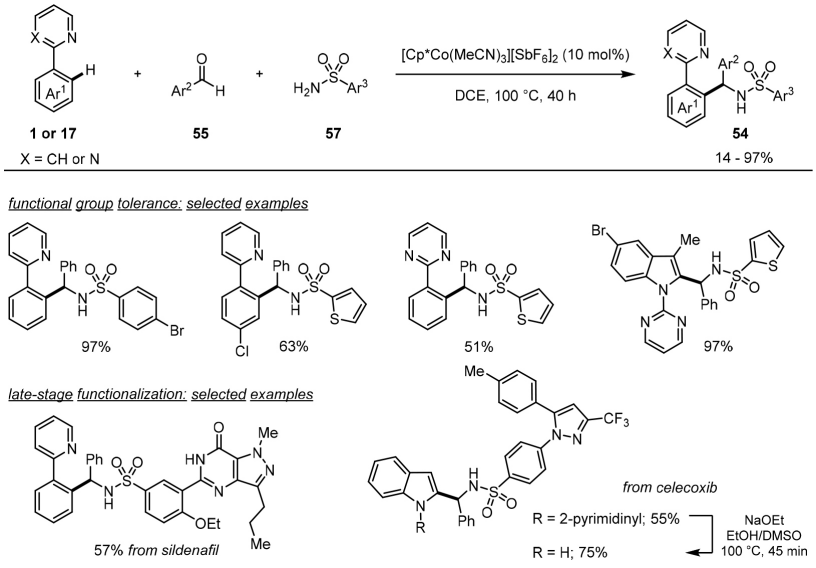

Scheme 19. Co-catalyzed C–H activation for a three-component Mannich-like coupling.

late-stage functionalization was demonstrated through the modification of complex drug molecules such as celecoxib, sildenafil.[105] Importantly, removal of 2-pyrimidyl directing group from the indole-containing products was also achieved, enabling further downstream functionalization of the indole scaffold.

5. Nickel Catalysis

Compared to palladium, nickel exhibits lower electronegativity (1.91 *vs.* 2.2) and a significantly lower standard reduction potential (–0.257 V *vs*. 0.951 V), rendering this 3d metal more readily engaged in oxidative processes, while reductive steps are comparatively less favorable. In addition, nickel binds strongly to π-acceptors ligands, and β-hydride elimination is generally slower for nickel than for palladium. Notably, nickel can also access one-electron redox pathways, enabling radical-type mechanisms.[15,106] Collectively, these electronic and reactivity features allow nickel to participate in diverse C–H activation manifolds and expand the range of compatible coupling partners for C–H functionalization.[107-109]

In the last decade, examples of Ni-catalyzed C–H activation focused basically on chelation assisted strategies. Besides exploring known directing groups, examples of new heterocycles capable of direct C–H activation were also reported. Strongly coordinating bidentate directing groups are the class of choice in most cases, because they show increased coordination affinity to the metal and, not only brings it into proximity to the ortho C–H bond but also influences the steric and electronic properties of the metal, stabilizing high valent intermediates produced along the catalytic cycle.[110,111]

Recently, this chelation-assisted Ni-catalyzed C–H strategy was extended to the aminoalkylation of aromatic benzamides (**25**) bearing an 8-aminoquinoline directing group, using β-iodoalkylamines (**58**) derived from α-amino acids as alkylating agent (Scheme 20).[112] Previously reported related reaction under palladium and ruthenium catalysis generally required acidic conditions.[113] Moreover, previously reported conditions for the alkylation of 25 using Ni-catalyzed C–H activation under the assistance of 8-aminoquinoline as a bidentate directing group[114] using alkyl halides (**16**) failed to furnish the aminoalkylated product (**59**). The authors then proposed a combination of Ni^{II}/Mn catalytic system, which may change the oxidative addition mechanism to a radical process involving Ni^{I} intermediates.[115,116] This catalytic system enabled the efficient aminoalkylation while suppressing β-hydride elimination, and preserving the stereochemical integrity of the chiral center. Although the requirement for stoichiometric manganese may represent a drawback, the reaction could also be conducted under reductant free conditions using a Ni^{0} catalyst, albeit with slightly diminished yields. This methodology allowed the incorporation of β-iodoalkylamines derived from natural amino acids, such as alanine, phenylalanine, tryptophan, and leucine, into benzamide framework. Moreover, this approach for C(sp^2)-H functionalization was successfully demonstrated in the late-stage aminoalkylation of natural products and biomolecules.

Kundu *et al.*[117] developed a Ni^{II}-catalyzed C–H activation protocol for the functionalization of benzamide (**60**) with aryl (**61**) and alkyl (**62**) iodides, assisted by a 8-aminoimidazo[1,2-*a*]pyridine (8-AIP) directing group (Scheme 21). As this heterocyclic scaffold is prevalent in bioactive molecules, its ability to act as an effective directing group is particularly attractive for late-stage functionalization applications. In this case, the strongly coordinating[111] ability of 8-AIP motif enabled directed over innate C–H activation, furnishing only the mono-functionalized products (**42**). Also, it facilitated the formation of high-valent Ni^{IV} intermediate via oxidative addition of organohalide[115] to Ni^{II} metallacycle formed by C–H activation process, without the need for additional ligands or external oxidants, and under only weakly basic conditions. Furthermore, the utility of this methodology was demonstrated through the site-selective late-stage

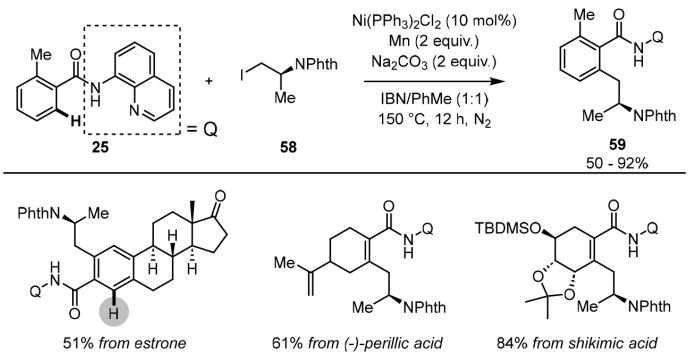

Scheme 20. Ni^{II}-catalyzed C–H aminoalkylation of benzamide (**25**) with β-iodoalkylamines (**58**).

arylation of an intermediate in route to antitumor derivatives (Scheme 21), where C–H activation *ortho* to the benzamide 8-AIP is achieved over the weakly coordinating acetanilide.

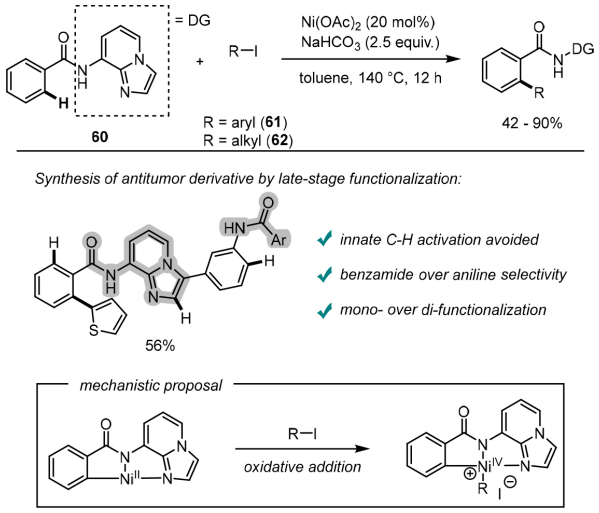

Scheme 21. 8-aminoimidazo[1,2-*a*]pyridine (8-AIP) as directing group for Ni^{II}-catalyzed C–H alkylation and arylation.

In 2022, a Ni^{II}-catalyzed, chelation assisted C–H activation of aromatic benzamides (**63**) was reported for the late-stage functionalization of commercial drugs bearing azole (**64**) units (Scheme 22).[118] The use of $NiCl_2/P(o\text{-tol})_3$ catalytic system in combination with a removable oxazoline-based bidentate directing group enabled an oxidative C–H/C–H coupling between aromatic benzamide (**63**) and azole heterocycles (**64**). Mechanistic investigations, including hydrogen/deuterium (H/D) exchange and kinetic isotope effect (KIE) experiments, suggested that C–H activation at the benzamide ring is irreversible, whereas cleavage of the acidic C–H bond at the azole ring is reversible, although neither step appears to be rate-determining. A range of directing groups was evaluated and, while pyrazol-based directing group (DG) proved similarly effective, other mono- and bidentate auxiliaries commonly found in bioactive molecules, such as sulfonamide and benzamides were ineffective. This limitation is, however, advantageous from a selectivity standpoint, as it enables site-selective late-stage C–H functionalization. Under the optimized conditions, the xanthine-derived drugs caffeine, pentoxifylline and doxofylline were coupled to aromatic benzamides in good yields (61-69%). Despite the clear advantage of avoiding prefunctionalization of the starting materials, the requirement for silver salts as oxidant raises sustainability concerns and may restrict the applicability of this methodology to more complex molecular scaffolds and to biomolecules.

In addition to benzamides, C–H activation of electron-rich aniline rings has also been explored in the context of late-stage functionalization. Based on previous report on monodentate pyrimidine-assisted Ni-catalyzed C–H activation,[119,120] Ackermann *et al.*[121] reported the first example of purine-directed C–H alkylation of aniline derivatives (**65**) under Ni^{II} catalysis (Scheme 23).[121] Notably, although the use of a *N*,*N*-bidentate ligand is not strictly required, it improves the yield of site-selective C–H activation of the aniline ring while suppressing activation of the more acidic C–H bond in the purine moiety. KIE and H/D exchange experiments suggested that the Ni^{II}-catalyzed C–H activation step is facile and not rate-determining, whereas radical scavenger experiments support a single-electron transfer pathway for C–Br bond cleavage. With respect to reaction scope, secondary and primary, cyclic and acyclic alkyl halides (**16**) were compatible with

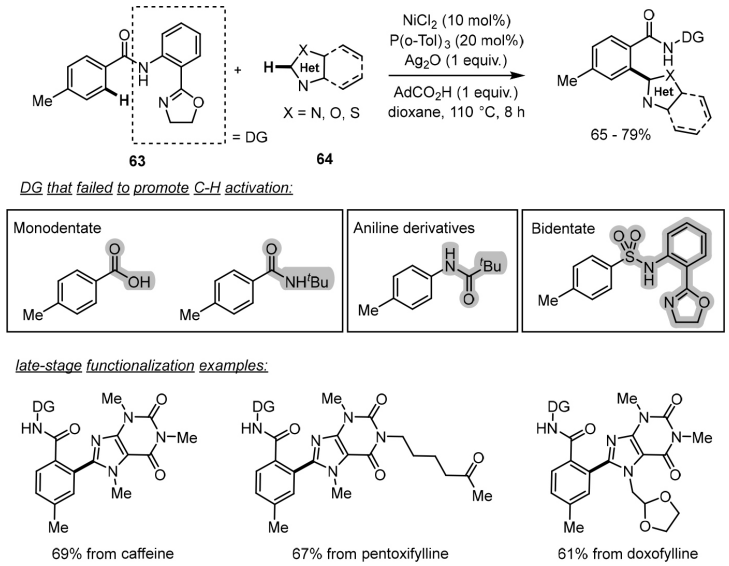

Scheme 22. Ni^{II}-catalyzed oxazoine-assisted oxidative C–H/C–H coupling between benzamide (**63**) and azoles (**64**).

this transformation, whereas tertiary alkyl halides failed to furnish the desired products. Under the optimized conditions, a purine nucleoside was successfully alkylated, and the protocol was further extended to fluorescent labeling of purine nucleobases. Notably, intermolecular competition experiment demonstrated a clear preference for purine over pyrimidine assistance[119] in the Ni^{II}-catalyzed C–H activation process, a feature that is particularly advantageous for potential applications in the late-stage functionalization of oligonucleosides. Despite these advances in site-selective C–H functionalization, the requirement for strongly basic reaction conditions may limit the applicability of this methodology to more complex, base-sensitive substrates.

Regioselective functionalization of naphthalenes is of great interest due to the presence of this motif in natural products and bioactive compounds.[122,123] While directed C–H functionalization typically favors *ortho* position, selective C8-H activation is particularly more challenging because of peri-strain.[124] The C8 alkylation of C1-substituted naphthalenes has already been reported using alkyl halides and alkenes; however, they require the use of noble metals.[125,126]

In this context, Zhang *et al.*[127] developed a Ni^{II}-catalyzed C–H activation strategy that enables highly regioselective C8 alkylation of naphthalene derivatives (**66**) using alkyl chlorides (**67**) as the alkylating agent (Scheme 24). The transformation employs a bidentate picolinamide directing group,[128] which is proposed to provide a favored bond angle for C8-H activation, while cobalt and zinc additives facilitate C–Cl bond activation via alkyl radical generation followed by addition to the nickelacyle formed upon directed C–H insertion. Notably, the method displays high selectivity for naphthalene framework, as benzene derivatives remain unreactive, and allows the incorporation of complex alkyl fragments derived from (–)-nopol and citronellol. Although the scope is constrained by reduced efficiency with sterically more demanding secondary chlorides (**67**), the requirement for strong basic conditions, and extended reaction times to reach moderate yields, the pronounced site- and chemoselectivity of this approach underscores its potential value for the functionalization of structurally complex molecules.

In 2022, Gou *et al.*[129] reported the first Ni-catalyzed difluoroalkylation of the *para* C–H position of *N*-substituted

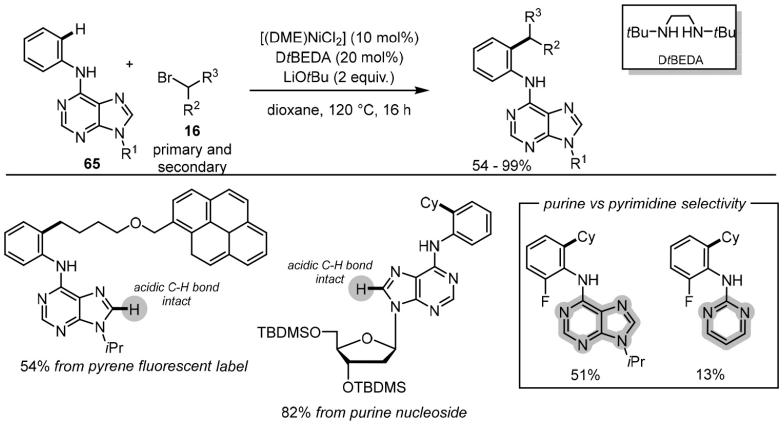

Scheme 23. Purine-directed C–H alkylation of aniline derivatives (**65**) under Ni^{II} catalysis.

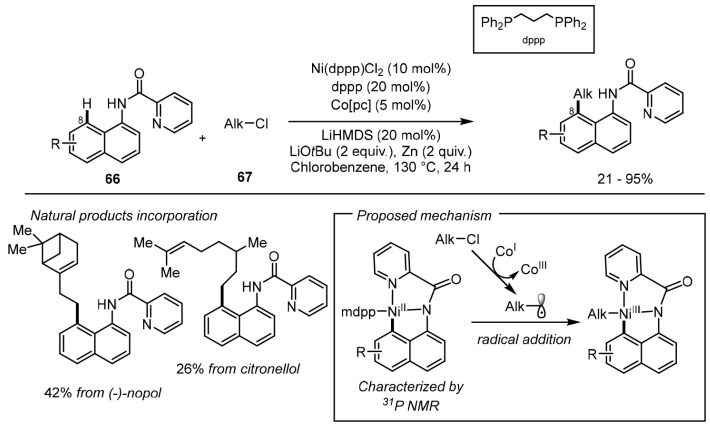

Scheme 24. Ni^{II}-catalyzed regioselective C8 alkylation of naphthalene (**66**) using alkyl chlorides.

anilines (**68**) (Scheme 25). This transformation proceeds with the assistance of a weakly-coordinating pivaloyl directing group,[111] using $Ni(OTf)_2$ and bulky 1,3-bis(diphenylphosphino)propane (DPPP) catalytic system, which enables initial *ortho* C–Ni bond formation. Rather than undergoing direct metal-centered coupling, the electrophilic[130] difluoroalkyl radical generated from (**69**) under the reaction conditions selectively adds to the more electron-rich and less sterically hindered *para* position of the aniline ring. The group used this approach to efficiently introduce the difluoroalkyl motifs into structurally complex molecules, including commercially available drugs such as ibuprofen and indomethacin, biomolecules such as pregabaline, and pesticides such as flutolanil. In the absence of pivaloyl directing group, however, the oxindole (**70**) formation is observed through an amide formation followed by intramolecular Ni-mediated radical cyclization reaction. Although other weakly-coordinating directing groups were also found to be compatible, this broad tolerance may be a drawback in site-selective late-stage functionalization.

6. Copper Catalysis

Copper salts are generally inexpensive and exhibit relatively low toxicity, contributing to their use in more sustainable catalytic methodologies. The most common and thermodynamically stable oxidation states are Cu^{I} and Cu^{II}. Cu^{I} characterized by a relatively small and positively charged metal center, is less electron-rich and nucleophilic than Pd^{0}, which influences its reactivity profile in C–H activation processes. In contrast, high-valent copper intermediates have been implicated in numerous oxidative transformations. Particularly, Cu^{III} intermediates are rather unstable and prone to facile reductive elimination, thereby enabling efficient C–X and C–C bond formation. Therefore, Cu-catalyzed C–H activation processes are often mechanistically intricate, involving the interplay of multiple oxidation states throughout the catalytic cycle.[131-134]

Over the past decade, significant advances in Cu-catalyzed C–H activation have centered on the development of strategies to achieve high levels of site- and chemo-selectivity, predominantly in the formation of C-heteroatom bonds. In addition to strongly coordinating bidentate directing groups, alternative approaches have emerged, including the implementation of transient directing groups and the exploitation of intrinsic electronic bias of specific C–H sites to guide selective functionalization.

The presence of metal-coordinating sites, such as heterocyclic rings, can pose significant challenges in late-stage C–H activation reactions. These functionalities may either poison the catalyst through strong coordination or act as unintended directing group, promoting undesired C–H activation pathways. Nevertheless, the bidentate auxiliary 8-aminoquinoline has already been demonstrated to allow selective *ortho* C–H amination of benzamides in the presence of heterocyclic motifs.[135]

In 2017, Yu *et al.*[136] exploited the affinity of Cu^{II} for a bidentate anionic oxazoline auxiliary to achieve *ortho* C–H activation of benzamide (**71**) proximal to this directing group, overriding competitive coordination from strongly binding heterocycles such as pyridine, pyrazole, pyrimidine, and triazoles (Scheme 26, right).[137] Under mildly basic aerobic conditions, the Cu^{II} system enabled late-stage amination of the antihypertensive drug telmisartan in good yield. With slightly modified conditions, other transformations, including hydroxylation, arylation and alkynylation, as well

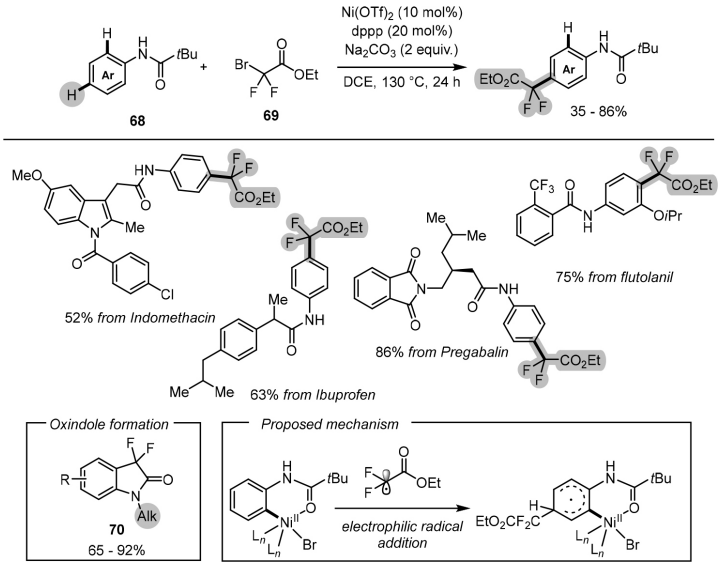

Scheme 25. Ni-catalyzed *para* C–H bond difluoroalkylation of *N*-substituted anilines.

as trifluoromethylation and -etherification could also be done. Notably, among several potentially reactive C–H bond sites, functionalization occurred exclusively adjacent to the oxazoline moiety, which could subsequently be removed, albeit under strongly acidic conditions.

Shortly after, the same group extended this strategy to the installation of unprotected amino groups, providing direct access to free anilines (**74**) (Scheme 26, left).[138] To perform this transformation, the authors proposed a switch to a Cu^{I} catalyst, enabling oxidative addition into oxime derivatives (**75**), followed by a rate-determining Cu^{III}-mediated, chelation assisted C–H activation. The methodology was likewise applied to the late-stage functionalization of telmisartan, affording the corresponding aniline after hydrolysis of the imine intermediate. Although the reaction proceeded under catalytic Cu^{I} loadings, significantly higher efficiency was achieved with stoichiometric copper, a limitation that reduces its suitability for drug development applications.

Indoles is an ubiquitous structural motifs found in natural products, biomolecules, and a wide range of bioactive compounds.[139,140] Because of the innate reactivity of the indole core, electrophilic C–H metallation preferentially occurs at the C3 position. In contrast, C2 metallation typically requires the presence of a chelation-assisting directing group located either on the nitrogen atom or at the C3 position, which in some cases can also enable activation of adjacent positions on the benzene ring.[141] Adjusting reaction conditions and using distinct directing group strategies therefore allow for selective funcionalization at different positions of the indole framework.

In 2020, Guo and co-workers[142] reported a directed Cu^{II}-catalyzed C–H activation strategy for the selective installation of a difluoroalkyl group at the C2 position of indoles (**1**) (Scheme 27a). A strongly coordination pyrimidyl group is essential to enable efficient C–H activation. The reaction proceeded through cyclic Cu^{II} intermediates that intercept difluoroalky radicals generated via oxidation of sodium difluoromethylsulfinate (**76**),[143] allowing the transformation to occur at relatively low temperatures. This protocol enabled the C2-difluoroalkylation of *N*-pyrimidyl indole-containing biomolecules, including melatonin, tryptophan and auxin. Despite the mild thermal conditions and high C2 selectivity, the requirement for strongly oxidative conditions to generate the difluoroalkyl radical limits the applicability of this method to more complex substrates bearing oxidation-sensitive functional groups. Later, simillar directed Cu^{II}-mediated C–H activation strategy employing a pyridine as directing group using commercially available thiols was also reported for selective C2 thiolation of the indole core of tryptophan.[144]

More recently, a transient directing group (TDG)[145-147] strategy has been merged to copper-mediated C–H activation to achieve sulfonylation at the less reactive C4 position of indoles (**77**) (Scheme 27b). *In situ* formation of a bidentate imine TDG occurs through condensation of a C3 aldehyde group on the indole with β-alanine (**78**), a process facilitated by the dehydrating properties of 1,1,1,3,3,3-hexafluoro-2-propanol (HFIP).[100] This imine TDG creates an appropriate binding site to promote six-membered Cu^{II} metallacycle (**79**) upon C4-H activation.[141] Notably, the transient nature of this directing group eliminates the need for separate installation and removal steps, thereby enhancing the step- and atom-economy of the overall C–H functionalization process. In addition to promoting C–H cleavage, Cu^{II} is also required for formation of sulfonyl radical from sodium aryl sulfinates (**80**).[148,149] In the absense of an external oxidant, stoichiometric amounts of copper are therefore necessary to achieve efficient sulfonylation. This approach was successfully applied to C4–H functionalization of indoles, enabling the synthesis of drug analogues using sildenafil- and valdecoxib-derived sulfinates as sulfonylating agents.

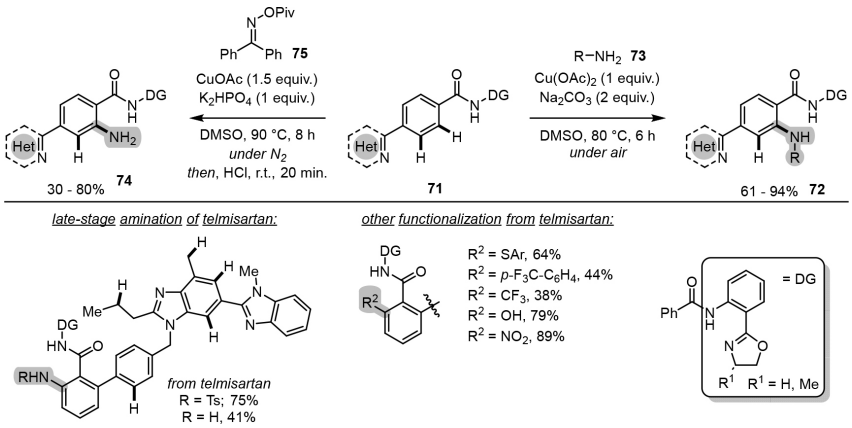

Scheme 26. Selective *ortho* C–H amination of benzamides (**71**) in the presence of heterocyclic motifs.

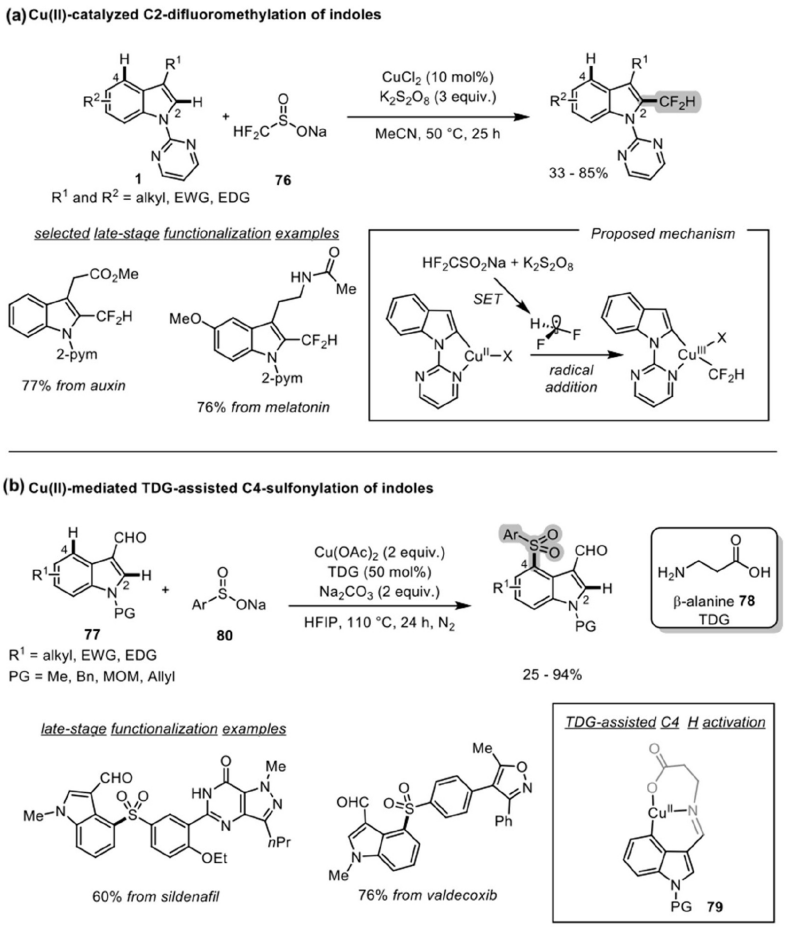

Scheme 27. Chelation-assisting directing group strategy for selective funcionalization at different positions of the indole framework. (a) Cu^{II}-catalyzed C2-H activation with the assistance of a *N*-heterocyclic directing group, (b) Cu^{II}-catalyzed C4-H activation with the assistance of an imine transient directing group. TDG: transient directing group.

Beyond the installation of exogenous directing groups, harnessing the electronic bias within a substrate represents an attractive strategy to achieve site-selectivity in late-stage C–H activation. The pyridine motif is prevalent in numerous FDA-approved pharmaceuticals and natural products.[150-152] Owing to its electron-defficient character and the Lewis basicity of the ring nitrogen, pyridine can readly coordinate to transition-metal catalyst, thereby acting as an internal directing group to promote C–H bond actvation in adjacent rings. Alternatively, dearomatization of the pyridine ring constitutes a complementary approach to invert its intrinsic reactivity, enabling subsequent C–H functionalization with electrophiles at the *meta* position.[153]

In 2022, Studer *et al.*[154] reported a redox-neutral dearomatization strategy that enables selective functionalization at the *meta* position of pyridines (**81**) through interception with radical or ionic nucleophiles. Shortly thereafter, the group extended this concept to a copper-catalyzed *meta*-arylation manifold. In this variant, a highly electrophilic aryl-Cu^{III} species, generated via oxidative addition of hypervalent iodine reagent (**82**) to Cu^{I}, undergoes selective addition to the more nucleophilic C3 position of an oxazinopyridine (**83**). Subsequent reductive elimination from Cu^{III}, followed by acidic hydrolisis, reestablish aromaticity to deliver the *meta*-arylated products (Scheme 28).[155]

Remarkably, the transformation proceeds with high chemoselectivity at the pyridine moiety, even in substrates bearing more nucleophilic heterocycles such as pyrole or thiophene. However, *ortho*-substituted pyridines proved unreactive under the optimized conditions. This approach was applied to the late-stage functionalization of natural product (±)-cotinine and commercially available drug ibuprofen. Despite its high *meta*-selectivity, the requirement for strong acidic conditions during rearomatization may limit its applicability to acid-sensitive, structurally more complex molecules. In addition, this dearomatization/rearomatization sequence raises concerns regarding atom economy, particularly in the context of developing more sustainable strategies for late-stage C–H functionalization.

Photoredox catalysis can be effectively merged with organometallic C–H activation to enable transformations

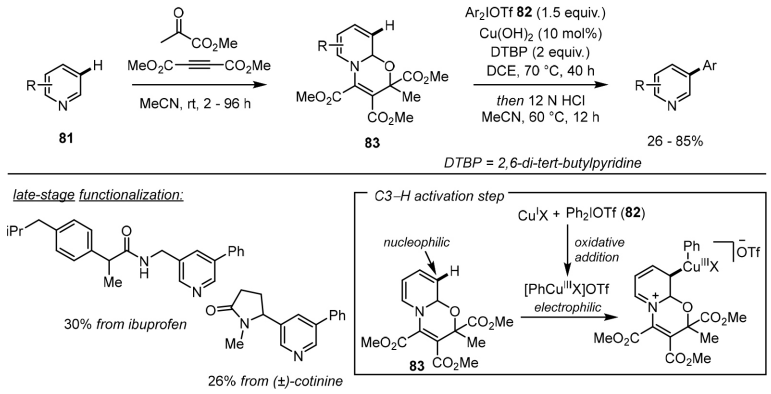

Scheme 28. Cu^{III}-catalyzed *meta* arylation of an oxazinopyridine (**83**).

under milder conditions, for example by replacing stoichometric oxidants typically required for the generation of high-valent metal intermediates, often at room temperature.[76,156] Copper-catayzed C–H arylation of benzazoles under photochemical conditions has been previously reported. However, these methods were largely limited to more acidic azoles, such as benzoxazoles and benzothiazoles, or required UV irradiation.[157,158]

Recently, Ackermann *et al.*[159] disclosed a Cu^{I}-catalyzed C–H arylation of less acidic benzimidazoles (**84**) using aryl iodides (**60**) as coupling partners under visible-light irradiation at room temperature (Scheme 29). In this system, coordination of the heterocyclic nitrogen increases the acidity of the C–H bond, facilitating Cu^{I}-mediated C–H cleavage. Concurrently, 10-phenylphenothiazine (PTH, $E^*_{1/2}$ = –2.1 V *vs.* saturated calomel electrode (SCE))[160] serves as a photoreductand, enabling the generation of aryl radical upon visible light excitation. Subsequent single electron oxidation of the Cu^{I} intermediate, followed by capture of the aryl radical, affords a Cu^{III} species that undergoes reductive elimination to furnish arylated products (**85**). Aryl iodides (**60**) bearing sensitive functionalities, including nitrile, chloro, and esters were well tolerated, highlighting the good functional group tolerance of this mild protocol. In addition, a variety of *N*-heterocycles such as benzoxazole, oxazole and thiazole were successfully arylated. The utility of this methodology was further demonstrated in the late-stage functionalization of structurally more complex iodides derivatives (**60**) of natural products, as well as in the gram-scale synthesis

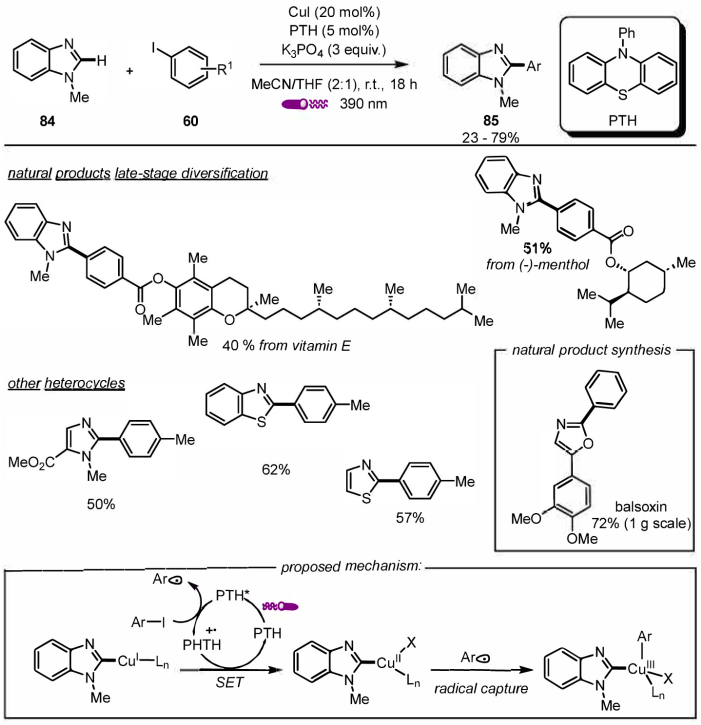

Scheme 29. Combination of photoredox and Cu^{I}-catalysis for C–H arylation of azoles.

of natural product balsoxin, highlighting its potential for applications in natural products diversification.

7. Conclusions and Perspectives

Late-stage functionalization (LSF) has unequivocally emerged as a valuable strategy for the rapid diversification of complex molecules, enabling the streamline synthesis and modification of bioactive compounds, natural products, and pharmaceuticals. Despite the significant advances in the development of 3d-metal-catalyzed C–H activation methodologies, examples involving the functionalization of more complex biomolecules, such as proteins and nucleic acids, as well as highly functionalized natural products, remain scarce across all the 3d metals discussed in this review.

A critical analysis of the key features and challenges associated with the use of 3d transition metals in the C–H functionalization of complex aromatic structures was provided in this review. In addition to more abundance, 3d metals often provide complementary reactivity to their noble metal congeners. Overall, irrespective of the metal employed, chelation-assisted C–H activation strategies dominate the field, while approaches that exploit the innate reactivity of aromatic C–H bonds in late-stage functionalization remain comparatively underdeveloped.

Among the 3d metals, cobalt and manganese are the most extensively explored, displaying notable tolerance toward halide functionalities, which is an advantageous feature for subsequent orthogonal transformations. However, their characteristic reactivity profiles largely favor addition pathways, which restrict the scope of coupling partners primarily to unsaturated systems such as alkenes and alkynes, thereby enabling alkenylation and alkylation reactions. In contrast, nickel has emerged as a preferred catalyst for arylation reactions and further broadens the scope of alkylation using alkyl halides. Copper, on the other hand, is most employed for carbon-heteroatom bond formation, whereas iron remains underrepresented in late-stage aromatic C–H functionalization, despite its potential to promote transformations under comparatively lower temperatures relative to its 4d counterpart.

Despite these advancements, significant opportunities remain for the development of new C–H activation methodologies using 3d metals. Greater emphasis on harnessing the innate reactivity of aromatic C–H bonds, especially in heteroaromatic systems, as well as the use of native functional groups as weakly coordinating directing groups, could enable improved reactivity and site-selectivity without the need of pre-installed auxiliaries. Additionally, the development of milder and more sustainable reaction conditions remains an important objective. In this context, coupling of metal catalysis with electrochemistry or light-mediated processes, as well as the use of lower temperatures and greener solvents, could expand the applicability of these methods to highly functionalized molecules and biomolecules, ultimately facilitating compatibility with aqueous and biologically relevant media.

Data Availability Statement

All data are available in the text.

Acknowledgments

The author gratefully acknowledges the UFRGS for providing research infrastructure.

Author Contributions

L. C. R. M. F.: conceptualization, data curation, writing (original draft, review & editing).

Lívia C. R. M. da Frota *earned her Pharmacy degree and PhD from the Federal Univesity of Rio de Janeiro (UFRJ) in 2016. She is currently an Assistant Professor at the Institute of Chemisrty, Federal University of Rio Grande do Sul (UFRGS). Her research interests focus on the development of synthetic methodologies based on C–H functionalizations, particularly using transition-metal catalysis for the synthesis of bioactive compounds and the modification of biomolecules.*

References

1. Börgel, J.; Ritter, T.; *Chem* **2020**, *6*, 1877. [Crossref]
2. Wencel-Delord, J.; Glorius, F.; *Nat. Chem.* **2013**, *5*, 369. [Crossref]
3. Cernak, T.; Dykstra, K. D.; Tyagarajan, S.; Vachal, P.; Krska, S. W.; *Chem. Soc. Rev.* **2016**, *45*, 546. [Crossref]
4. Guillemard, L.; Kaplaneris, N.; Ackermann, L.; Johansson, M. J.; *Nat. Rev. Chem.* **2021**, *5*, 522. [Crossref]
5. Docherty, J. H.; Lister, T. M.; Mcarthur, G.; Findlay, M. T.; Domingo-Legarda, P.; Kenyon, J.; Choudhary, S.; Larrosa, I.; *Chem. Rev.* **2023**, *123*, 7692. [Crossref]
6. Shang, W.; Sun, H.; Chen, W.; Liu, J.; *Green Synth. Catal.* **2023**, *4*, 104. [Crossref]
7. Rej, S.; Ano, Y.; Chatani, N.; *Chem. Rev.* **2020**, *120*, 1788. [Crossref]

8. Ali, W.; Oliver, G. A.; Werz, D. B.; Maiti, D.; *Chem. Soc. Rev.* **2024**, *53*, 9904. [Crossref]
9. Tang, H.; Zhou, B.; Huang, X. R.; Wang, C.; Yao, J.; Chen, H.; *ACS Catal.* **2014**, *4*, 649. [Crossref]
10. Tang, H.; Huang, X. R.; Yao, J.; Chen, H.; *J. Org. Chem.* **2015**, *80*, 4672. [Crossref]
11. He, J.; Wasa, M.; Chan, K. S. L.; Shao, Q.; Yu, J. Q.; *Chem. Rev.* **2017**, *117*, 8754. [Crossref]
12. Josephitis, C. M.; Nguyen, H. M. H.; McNally, A.; *Chem. Rev.* **2023**, *123*, 7655. [Crossref]
13. Gandeepan, P.; Müller, T.; Zell, D.; Cera, G.; Warratz, S.; Ackermann, L.; *Chem. Rev.* **2019**, *119*, 2192. [Crossref]
14. Bera, A.; Kabadwal, L. M.; Bera, S.; Banerjee, D.; *Chem. Commun.* **2022**, *58*, 10. [Crossref]
15. Ananikov, V. P.; *ACS Catal.* **2015**, *5*, 1964. [Crossref]
16. Jagtap, R. A.; Punji, B.; *Asian J. Org. Chem.* **2020**, *9*, 326. [Crossref]
17. Ashraf, B.; Kanwal, A.; Ahmad, M.; Rasool, N.; Malik, A.; Arshad, M.; Suleman, M.; *ChemistrySelect* **2025**, *10*, e03379. [Crossref]
18. Mohite, S. B.; Mirza, Y. K.; Bera, P. S.; Nadigar, S.; Yugendhar, S.; Karpoormath, R.; Bera, M.; *Chem. - Eur. J.* **2025**, *31*, e202403032. [Crossref]
19. Park, Y.; Park, J.; Lee, Y. H.; Son, J.; *Bull. Korean Chem. Soc.* **2025**, *46*, 622. [Crossref]
20. Harry, N. A.; Saranya, S.; Ujwaldev, S. M.; Anilkumar, G.; *Catal. Sci. Technol.* **2019**, *9*, 1726. [Crossref]
21. Serpier, F.; Pan, F.; Ham, W. S.; Jacq, J.; Genicot, C.; Ritter, T.; *Angew. Chem., Int. Ed.* **2018**, *130*, 10857. [Crossref]
22. Ghosh, P.; Kwon, N. Y.; Byun, Y.; Mishra, N. K.; Park, J. S.; Kim, I. S.; *ACS Catal.* **2022**, *12*, 15707. [Crossref]
23. Yamamoto, K.; Li, J.; Garber, J. A. O.; Rolfes, J. D.; Boursalian, G. B.; Borghs, J. C.; Genicot, C.; Jacq, J.; Van Gastel, M.; Neese, F.; Ritter, T.; *Nature* **2018**, *554*, 511. [Crossref]
24. Al-Afyouni, M. H.; Krishnan, V. M.; Arman, H. D.; Tonzetich, Z. J.; *Organometallics* **2015**, *34*, 5088. [Crossref]
25. Ahmed, N.; *J. Organomet. Chem.* **2024**, *1009*, 123071. [Crossref]
26. White, M. C.; Zhao, J.; *J. Am. Chem. Soc.* **2018**, *140*, 13988. [Crossref]
27. Cano, R.; Mackey, K.; McGlacken, G. P.; *Catal. Sci. Technol.* **2018**, *8*, 1251. [Crossref]
28. Anusree, G.; Devi, P. S.; Anilkumar, G.; *Adv. Synth. Catal.* **2024**, *366*, 3963. [Crossref]
29. Liu, W.; Ackermann, L.; *ACS Catal.* **2016**, *6*, 3743. [Crossref]
30. Hu, Y.; Zhou, B.; Wang, C.; *Acc. Chem. Res.* **2018**, *51*, 816. [Crossref]
31. Maayuri, R.; Gandeepan, P.; *Org. Biomol. Chem.* **2023**, *21*, 441. [Crossref]
32. Ruan, Z.; Sauermann, N.; Manoni, E.; Ackermann, L.; *Angew. Chem., Int. Ed.* **2017**, *56*, 3172. [Crossref]
33. Wang, H.; Pesciaioli, F.; Oliveira, J. C. A.; Warratz, S.; Ackermann, L.; *Angew. Chem., Int. Ed.* **2017**, *56*, 15063. [Crossref]
34. Kaplaneris, N.; Kaltenhäuser, F.; Sirvinskaite, G.; Fan, S.; de Oliveira, T.; Conradi, L.-C.; Ackermann, L.; *Sci. Adv.* **2021**, *7*, eabe6202. [Crossref]
35. Kaplaneris, N.; Son, J.; Mendive-Tapia, L.; Kopp, A.; Barth, N. D.; Maksso, I.; Vendrell, M.; Ackermann, L.; *Nat. Commun.* **2021**, *12*, 3389. [Crossref]
36. Oyama, T.; Mendive-Tapia, L.; Cowell, V.; Kopp, A.; Vendrell, M.; Ackermann, L.; *Chem. Sci.* **2023**, *14*, 5728. [Crossref]
37. Jei, B. B.; Yang, L.; Ackermann, L.; *Chem. - Eur. J.* **2022**, *28*, e202200811. [Crossref]
38. Kopp, A.; Oyama, T.; Ackermann, L.; *Chem. Commun.* **2024**, *60*, 5423. [Crossref]
39. Bhat, U. V.; Martis, G. J.; Chikkanna, D.; Gaonkar, S. L.; *J. Chem.* **2025**, *2025*, 9002020. [Crossref]
40. Cheng, Y.; Li, G.; Liu, Y.; Shi, Y.; Gao, G.; Wu, D.; Lan, J.; You, J.; *J. Am. Chem. Soc.* **2016**, *138*, 4730. [Crossref]
41. Brückl, T.; Baxter, R. D.; Ishihara, Y.; Baran, P. S.; *Acc. Chem. Res.* **2012**, *45*, 826. [Crossref]
42. Liu, L.; Durai, M.; Doucet, H.; *Eur. J. Org. Chem.* **2022**, *2022*, e202200007. [Crossref]
43. Yang, Z.; Yu, J.-T.; Pan, C.; *Org. Biomol. Chem.* **2022**, *20*, 7746. [Crossref]
44. Das, K. K.; Ghosh, A. K.; Hajra, A.; *RSC Adv.* **2022**, *12*, 19412. [Crossref]
45. Wang, C.; Wang, A.; Rueping, M.; *Angew. Chem., Int. Ed.* **2017**, *56*, 9935. [Crossref]
46. Matesanz, D. G.; Gamarra, L.; del Campo, T. M.; Almendros, P.; Cembellín, S.; *ACS Catal.* **2023**, *13*, 14523. [Crossref]
47. Blaha, I.; Weber, S.; Dulger, R.; Veiros, L. F.; Kirchner, K.; *ACS Catal.* **2024**, *14*, 13174. [Crossref]
48. Wang, H.; Lorion, M. M.; Ackermann, L.; *Angew. Chem., Int. Ed.* **2017**, *56*, 6339. [Crossref]
49. Wencel-Delord, J.; Colobert, F.; *Org. Chem. Front.* **2016**, *3*, 394. [Crossref]
50. Ni, J.; Zhao, H.; Zhang, A.; *Org. Lett.* **2017**, *19*, 3159. [Crossref]
51. Kaplaneris, N.; Rogge, T.; Yin, R.; Wang, H.; Sirvinskaite, G.; Ackermann, L.; *Angew. Chem., Int. Ed.* **2019**, *58*, 3476. [Crossref]
52. Struwe, J.; Oyama, T.; Gallou, F.; Ackermann, L.; *Synlett* **2024**, *35*, 903. [Crossref]
53. Liu, W.; Cera, G.; Oliveira, J. C. A.; Shen, Z.; Ackermann, L.; *Chem. Eur. J.* **2017**, *23*, 11524. [Crossref]
54. Shen, Z.; Huang, H.; Zhu, C.; Warratz, S.; Ackermann, L.; *Org. Lett.* **2019**, *21*, 571. [Crossref]
55. Verma, S. K.; Punji, B.; *Chem. Asian J.* **2022**, *17*, e202200103. [Crossref]

56. Rana, S.; Biswas, J. P.; Paul, S.; Paik, A.; Maiti, D.; *Chem. Soc. Rev.* **2021**, *50*, 243. [Crossref]
57. Shang, R.; Ilies, L.; Nakamura, E.; *Chem. Rev.* **2017**, *117*, 9086. [Crossref]
58. Mo, J.; Messinis, A. M.; Li, J.; Warratz, S.; Ackermann, L.; *Acc. Chem. Res.* **2024**, *57*, 10. [Crossref]
59. Tang, S.; Eisenstein, O.; Nakao, Y.; Sakaki, S.; *Organometallics* **2017**, *36*, 2761. [Crossref]
60. Zhang, Z. J.; Golling, S.; Cattani, S.; Chen, X.; Ackermann, L.; *J. Am. Chem. Soc.* **2025**, *147*, 6897. [Crossref]
61. Cattani, S.; Cordovani, F.; Balestri, D.; Oliveira, J. C. A.; Peters, S. E.; Ackermann, L.; Cera, G.; *Org. Lett.* **2025**, *27*, 7950. [Crossref]
62. Zell, D.; Bursch, M.; Müller, V.; Grimme, S.; Ackermann, L.; *Angew. Chem., Int. Ed.* **2017**, *56*, 10378. [Crossref]
63. Grigg, R.; Savic, V.; *Tetrahedron Lett.* **1997**, *38*, 5737. [Crossref]
64. Borah, A. J.; Shi, Z.; *Chem. Commun.* **2017**, *53*, 3945. [Crossref]
65. Kumar, D. V.; Sundararaju, B.; *J. Org. Chem.* **2024**, *89*, 10087. [Crossref]
66. Moselage, M.; Li, J.; Ackermann, L.; *ACS Catal.* **2016**, *6*, 498. [Crossref]
67. Wei, D.; Zhu, X.; Niu, J. L.; Song, M. P.; *ChemCatChem* **2016**, *8*, 1242. [Crossref]
68. Anjali, S.; Devi, P. S.; Anilkumar, G.; *Chem. Rec.* **2025**, *25*, e202500009. [Crossref]
69. Barsu, N.; Kalsi, D.; Sundararaju, B.; *Catal. Sci. Technol.* **2018**, *8*, 5963. [Crossref]
70. Friis, S. D.; Lindhardt, A. T.; Skrydstrup, T.; *Acc. Chem. Res.* **2016**, *49*, 594. [Crossref]
71. Grigorjeva, L.; Daugulis, O.; *Org. Lett.* **2014**, *16*, 4688. [Crossref]
72. Lukasevics, L.; Cizikovs, A.; Grigorjeva, L.; *Org. Lett.* **2021**, *23*, 2748. [Crossref]
73. Shankar, M.; Saha, A.; Sau, S.; Ghosh, A.; Gandon, V.; Sahoo, A. K.; *Chem. Sci.* **2021**, *12*, 6393. [Crossref]
74. Ochiai, S.; Sakai, A.; Usuki, Y.; Kang, B.; Shinada, T.; Satoh, T.; *Chem. Lett.* **2021**, *50*, 585. [Crossref]
75. Sharma, N.; Saha, R.; Parveen, N.; Sekar, G.; *Adv. Synth. Catal.* **2017**, *359*, 1947. [Crossref]
76. Dwivedi, V.; Kalsi, D.; Sundararaju, B.; *ChemCatChem* **2019**, *11*, 5160. [Crossref]
77. Baroliya, P. K.; Dhaker, M.; Panja, S.; Al-Thabaiti, S. A.; Albukhari, S. M.; Alsulami, Q. A.; Dutta, A.; Maiti, D.; *ChemSusChem* **2023**, *16*, e202202201. [Crossref]
78. Dhawa, U.; Kaplaneris, N.; Ackermann, L.; *Org. Chem. Front.* **2021**, *8*, 4886. [Crossref]
79. Huang, Y. H.; Dong, L.; *Adv. Synth. Catal.* **2023**, *365*, 23. [Crossref]
80. Khot, N. P.; Deo, N. K.; Kapur, M.; *Chem. Commun.* **2022**, *58*, 13967. [Crossref]
81. Cui, S.; Zhang, Y.; Wang, D.; Wu, Q.; *Chem. Sci.* **2013**, *4*, 3912. [Crossref]
82. Yu, D.; Gensch, T.; de Azambuja, F.; Vásquez-Céspedes, S.; Glorius, F.; *J. Am. Chem. Soc.* **2014**, *136*, 17722. [Crossref]
83. Lorion, M. M.; Kaplaneris, N.; Son, J.; Kuniyil, R.; Ackermann, L.; *Angew. Chem., Int. Ed.* **2019**, *58*, 1684. [Crossref]
84. Hu, H.; Xu, W. H.; Kang, W. X.; Sun, W.; Sun, R.; Wei, X. H.; Sun, M.; *Org. Chem. Front.* **2021**, *8*, 4459. [Crossref]
85. Saha, S.; Bhattacharyya, H.; Karjee, P.; Debnath, B.; Verma, K.; Punniyamurthy, T.; *Chem. Commun.* **2023**, *59*, 14173. [Crossref]
86. Halskov, K. S.; Witten, M. R.; Hoang, G. L.; Mercado, B. Q.; Ellman, J. A.; *Org. Lett.* **2018**, *20*, 2464. [Crossref]
87. Vaitla, J.; Bayer, A.; Hopmann, K. H.; *Angew. Chem., Int. Ed.* **2017**, *56*, 4277. [Crossref]
88. Oh, H.; Han, S.; Pandey, A. K.; Han, S. H.; Mishra, N. K.; Kim, S.; Chun, R.; Kim, H. S.; Park, J.; Kim, I. S.; *J. Org. Chem.* **2018**, *83*, 4070. [Crossref]
89. Barday, M.; Janot, C.; Halcovitch, N. R.; Muir, J.; Aïssa, C.; *Angew. Chem., Int. Ed.* **2017**, *56*, 13117. [Crossref]
90. Friis, S. D.; Johansson, M. J.; Ackermann, L.; *Nat. Chem.* **2020**, *12*, 511. [Crossref]
91. Li, C.; Sotorrios, L.; Boaler, P. J.; Olikauskas, V.; Amico, M.; García-Domínguez, A.; Leach, A. G.; Lloyd-Jones, G. C.; *J. Am. Chem. Soc.* **2025**, *147*, 38237. [Crossref]
92. Shi, Y.; Yuan, Y.; Li, J.; Yang, J.; Zhang, J.; *J. Am. Chem. Soc.* **2024**, *146*, 17580. [Crossref]
93. Aynetdinova, D.; Callens, M. C.; Hicks, H. B.; Poh, C. Y. X.; Shennan, B. D. A.; Boyd, A. M.; Lim, Z. H.; Leitch, J. A.; Dixon, D. J.; *Chem. Soc. Rev.* **2021**, *50*, 5517. [Crossref]
94. Bera, S. S.; Maji, M. S.; *Org. Lett.* **2020**, *22*, 2615. [Crossref]
95. Yang, J.; Hu, X.; Liu, Z.; Li, X.; Dong, Y.; Liu, G.; *Chem. Commun.* **2019**, *55*, 13840. [Crossref]
96. Jiang, Q.; Han, P.; Lu, M.; Feng, T.; Wang, J.; *Org. Chem. Front.* **2026**, *13*, 501. [Crossref]
97. Barsu, N.; Sen, M.; Premkumar, J. R.; Sundararaju, B.; *Chem. Commun.* **2016**, *52*, 1338. [Crossref]
98. Stephens, D. E.; Lakey-Beitia, J.; Atesin, A. C.; Ateşin, T. A.; Chavez, G.; Arman, H. D.; Larionov, O. V.; *ACS Catal.* **2015**, *5*, 167. [Crossref]
99. Mandal, S.; Paul, T.; Karjee, P.; Barman, M.; Punniyamurthy, T.; *Org. Lett.* **2023**, *25*, 7805. [Crossref]
100. Motiwala, H. F.; Armaly, A. M.; Cacioppo, J. G.; Coombs, T. C.; Koehn, K. R. K.; Norwood, V. M.; Aubé, J.; *Chem. Rev.* **2022**, *122*, 12544. [Crossref]
101. Sakthivel, K.; Gana, R. J.; Shoji, T.; Takenaga, N.; Dohi, T.; Singh, F. V.; *Front. Chem.* **2023**, *11*, 1217744. [Crossref]
102. Wan, J.-P.; Gan, L.; Liu, Y.; *Org. Biomol. Chem.* **2017**, *15*, 9031. [Crossref]
103. Whitehurst, W. G.; Kim, J.; Koenig, S. G.; Chirik, P. J.; *J. Am. Chem. Soc.* **2022**, *144*, 4530. [Crossref]

104. Olu-Igbiloba, O. A.; Sitzmann, H.; Manolikakes, G.; *J. Org. Chem.* **2024**, *89*, 6903. [Crossref]
105. Olu-Igbiloba, O. A.; Sitzmann, H.; Manolikakes, G.; *Synthesis* **2025**, *57*, 1015. [Crossref]
106. Diccianni, J.; Lin, Q.; Diao, T.; *Acc. Chem. Res.* **2020**, *53*, 906. [Crossref]
107. Chernyshev, V. M.; Ananikov, V. P.; *ACS Catal.* **2022**, *12*, 1180. [Crossref]
108. Tasker, S. Z.; Standley, E. A.; Jamison, T. F.; *Nature* **2014**, *509*, 299. [Crossref]
109. Khamrai, A.; Ghosh, S.; Ganesh, V.; *Chem. Commun.* **2025**, *61*, 3037. [Crossref]
110. Clevenger, A. L.; Stolley, R. M.; Aderibigbe, J.; Louie, J.; *Chem. Rev.* **2020**, *120*, 6124. [Crossref]
111. Mandal, R.; Garai, B.; Sundararaju, B.; *ACS Catal.* **2022**, *12*, 3452. [Crossref]
112. Tian, J. S.; Li, R. Q.; Liu, D. Y.; Tan, J.; Yang, Y. X.; Loh, T. P.; *Org. Chem. Front.* **2026**, *13*, 210. [Crossref]
113. Ankade, S. B.; Shabade, A. B.; Soni, V.; Punji, B.; *ACS Catal.* **2021**, *11*, 3268. [Crossref]
114. Aihara, Y.; Chatani, N.; *J. Am. Chem. Soc.* **2013**, *135*, 5308. [Crossref]
115. Omer, H. M.; Liu, P.; *J. Am. Chem. Soc.* **2017**, *139*, 9909. [Crossref]
116. Kehoe, R.; Mahadevan, M.; Manzoor, A.; McMurray, G.; Wienefeld, P.; Baird, M. C.; Budzelaar, P. H. M.; *Organometallics* **2018**, *37*, 2450. [Crossref]
117. Joardar, S. K.; Rao, G. P.; Soumya, J.; Midya, S.; Das, R.; Kundu, M.; Kundu, T.; *Synthesis* **2025**, *57*, 2207. [Crossref]
118. Sarkar, T.; Maharana, P. K.; Roy, S.; Punniyamurthy, T.; *Chem. Commun.* **2022**, *58*, 5980. [Crossref]
119. Ruan, Z.; Lackner, S.; Ackermann, L.; *ACS Catal.* **2016**, *6*, 4690. [Crossref]
120. Ruan, Z.; Lackner, S.; Ackermann, L.; *Angew. Chem., Int. Ed.* **2016**, *55*, 3153. [Crossref]
121. Ruan, Z.; Ghorai, D.; Zanoni, G.; Ackermann, L.; *Chem. Commun.* **2017**, *53*, 9113. [Crossref]
122. Makar, S.; Saha, T.; Singh, S. K.; *Eur. J. Med. Chem.* **2019**, *161*, 252. [Crossref]
123. Silva, O.; Gomes, E. T.; *J. Nat. Prod.* **2003**, *66*, 447. [Crossref]
124. Balasubramaniyan, V.; *Chem. Rev.* **1966**, *66*, 567. [Crossref]
125. Huang, L.; Sun, X.; Li, Q.; Qi, C.; *J. Org. Chem.* **2014**, *79*, 6720. [Crossref]
126. Rej, S.; Chatani, N.; *ACS Catal.* **2018**, *8*, 6699. [Crossref]
127. Song, W.; Shi, X.; Li, W.; Yao, S.; Mao, Y.; Zhang, Y.; *Chin. J. Chem.* **2025**, *43*, 1121. [Crossref]
128. Prévost, S.; *ChemPlusChem* **2020**, *85*, 476. [Crossref]
129. Gou, Q.; Chen, Q.; Tan, Q.; Zhu, M.; Huang, H.; Deng, M.; Yi, W.; He, S.; *Org. Lett.* **2022**, *24*, 3549. [Crossref]
130. Parsaee, F.; Senarathna, M. C.; Kannangara, P. B.; Alexander, S. N.; Arche, P. D. E.; Welin, E. R.; *Nat. Rev. Chem.* **2021**, *5*, 486. [Crossref]
131. Wendlandt, A. E.; Suess, A. M.; Stahl, S. S.; *Angew. Chem., Int. Ed.* **2011**, *50*, 11062. [Crossref]
132. Guo, X.; Gu, D.; Wu, Z.; Zhang, W.; *Chem. Rev.* **2015**, *115*, 1622. [Crossref]
133. Beletskaya, I. P.; Cheprakov, A. V.; *Organometallics* **2012**, *31*, 7753. [Crossref]
134. Joseph, P. J. A.; Priyadarshini, S.; *Org. Process Res. Dev.* **2017**, *21*, 1889. [Crossref]
135. Roane, J.; Daugulis, O.; *J. Am. Chem. Soc.* **2016**, *138*, 4601. [Crossref]
136. Shang, M.; Sun, S.-Z.; Dai, H.-X.; Yu, J.-Q.; *J. Am. Chem. Soc.* **2014**, *136*, 3354. [Crossref]
137. Shang, M.; Wang, M.; Saint-Denis, T. G.; Li, M.; Dai, H.; Yu, J.-Q.; *Angew. Chem., Int. Ed.* **2017**, *56*, 5317. [Crossref]
138. Xu, L.-L.; Wang, X.; Ma, B.; Yin, M.-X.; Lin, H.-X.; Dai, H.-X.; Yu, J.-Q.; *Chem. Sci.* **2018**, *9*, 5160. [Crossref]
139. Babalola, B. A.; Malik, M.; Olowokere, O.; Adebesin, A.; Sharma, L.; *Eur. J. Med. Chem. Rep.* **2025**, *13*, 100252. [Crossref]
140. Umer, S. M.; Solangi, M.; Khan, K. M.; Saleem, R. S. Z.; *Molecules* **2022**, *27*, 7586. [Crossref]
141. Kumar, P.; Nagtilak, P. J.; Kapur, M.; *New J. Chem.* **2021**, *45*, 13692. [Crossref]
142. Zhang, D.; Fang, Z.; Cai, J.; Liu, C.; He, W.; Duan, J.; Qin, N.; Yang, Z.; Guo, K.; *Chem. Commun.* **2020**, *56*, 8119. [Crossref]
143. Sap, J. B. I.; Meyer, C. F.; Straathof, N. J. W.; Iwumene, N.; Ende, C. W.; Trabanco, A. A.; Gouverneur, V.; *Chem. Soc. Rev.* **2021**, *50*, 8214. [Crossref]
144. Ma, W.; Xu, Y.; Gu, Q.; Zheng, T.; Gu, L.; *Eur. J. Org. Chem.* **2024**, *27*, e202301253. [Crossref]
145. Gandeepan, P.; Ackermann, L.; *Chem* **2018**, *4*, 199. [Crossref]
146. Bhattacharya, T.; Pimparkar, S.; Maiti, D.; *RSC Adv.* **2018**, *8*, 19456. [Crossref]
147. Higham, J. I.; Ma, T.; Bull, J. A.; *Chem. - Eur. J.* **2024**, *30*, e202400345. [Crossref]
148. Higham, J. I.; Ma, T.-K.; Bull, J. A.; *Org. Lett.* **2023**, *25*, 5285. [Crossref]
149. Ma, T.-K.; Begg, C. S.; Bull, J. A.; *ACS Electrochem.* **2025**, *1*, 1863. [Crossref]
150. Naushad, E.; Thangaraj, S.; *Exploring Chemistry with Pyridine Derivatives*; IntechOpen: London, UK, 2023. [Link] accessed in June 2026
151. Bhutani, P.; Joshi, G.; Raja, N.; Bachhav, N.; Rajanna, P. K.; Bhutani, H.; Paul, A. T.; Kumar, R.; *J. Med. Chem.* **2021**, *64*, 2339. [Crossref]
152. de la Torre, B. G.; Albericio, F.; *Molecules* **2025**, *30*, 482. [Crossref]

153. Josephitis, C. M.; Nguyen, H. M. H.; McNally, A.; *Chem. Rev.* **2023**, *123*, 7655. [Crossref]
154. Cao, H.; Cheng, Q.; Studer, A.; *Science* **2022**, *378*, 779. [Crossref]
155. Guo, S. M.; Xu, P.; Studer, A.; *Angew. Chem., Int. Ed.* **2024**, *63*, e202405385. [Crossref]
156. Gensch, T.; Hopkinson, M. N.; Glorius, F.; Wencel-Delord, J.; *Chem. Soc. Rev.* **2016**, *45*, 2900. [Crossref]
157. Yang, F.; Koeller, J.; Ackermann, L.; *Angew. Chem., Int. Ed.* **2016**, *55*, 4759. [Crossref]
158. Ma, X.; Zhang, G.; *Chin. J. Chem.* **2020**, *38*, 1299. [Crossref]
159. Trienes, S.; Xu, J.; Ackermann, L.; *Chem. Sci.* **2024**, *15*, 7293. [Crossref]
160. Discekici, E. H.; Treat, N. J.; Poelma, S. O.; Mattson, K. M.; Hudson, Z. M.; Luo, Y.; Hawker, C. J.; de Alaniz, J. R.; *Chem. Commun.* **2015**, *51*, 11705. [Crossref]

Submitted: April 15, 2026
Final version online: June 12, 2026